CO-IMPLANTATION AND DRY-ETCH DAMAGE RECOVERY BY PLASMA NITRIDATION IN GaN

BY

DONALD G. KENT III

A THESIS PRESENTED TO THE GRADUATE SCHOOL
OF THE UNIVERSITY OF FLORIDA IN PARTIAL FULFILLMENT
OF THE REQUIREMENTS FOR THE DEGREE OF
MASTER OF SCIENCE

UNIVERSITY OF FLORIDA

2001

ACKNOWLEDGEMENTS

Most importantly, sincerest thanks go to my advisor Dr. Stephen J. Pearton. I deeply appreciate the educational and professional environment that being associated with him has afforded me. Without his guidance and direction this research would not have been possible.

Also I would also like to thank the members of my committee, Dr. Cammy R. Abernathy and Dr. Fan Ren, for their time and the use of their facilities and equipment. I would like to recognize two of their graduate students M.E. Overberg and A.P. Zhang for their kind assistance and expert help.

Many thanks to my fellow Pearton research group member Kyu-pil Lee, who is an 'excellent engineer'; he is also a great mentor and friend.

Finally, I would like to thank my wife, parents, and family for their love, support, and encouragement throughout the past several years. Without their understanding and patience the road less traveled would want for one more pair of feet.

TABLE OF CONTENTS

Page

ACKNOWLEDGEMENTS ii

LIST OF TABLES v

LIST OF FIGURES vi

ABSTRACT x

CHAPTERS

1 INTRODUCTION 1

1.1 GaN Applications 1
1.2 GaN Material Issues 3

2 BACKGROUND INFORMATION 11

2.1 Ion implantation 11
2.2 Etching of GaN 26

3 ELECTRICAL EFFECTS OF N2 PLASMA EXPOSURE
ON DRY-ETCH DAMAGE IN P- AND N- GaN SCHOTTKY
DIODES 38

3.1 Materials and Methods 38
3.2 Results and Discussion 40

4 CO-IMPLANTATION OF Be + O AND Mg + O INTO GaN 51

4.1 Materials and Methods 51
4.2 Results and Discussion 54

5 SUMMARY 63

APPENDIX ……………………………………………………………….. 65

LIST OF REFERENCES ……….…………………………………………… 71

BIOGRAPHICAL SKETCH ………………………………………….. 80

LIST OF TABLES

Table Page

1. Comparison of sapphire and SiC: the two most popular substrate materials for heteroepitaxal growth on GaN, showing lattice parameter and thermal expansion coefficient 5

2. Shallow acceptor and donor levels in GaN..................................... 9

3. Summary of electrical data for Be + O (a) and Mg + O (b) implanted samples in GaN... 55

4. Ion range statistics of Be in GaN... 65

5. Ion range statistics of Mg in GaN.. 67

6. Ion range statistics of O in GaN.. 69

LIST OF FIGURES

Figure page

1. GaN LED market history (top). Market forecast for GaN based optoelectronic and electronic devices (bottom)………………. 2

2. Chronological representation of the development of the performance of GaN- and GaAs-based light emitting diodes…………….. 4

3. TEM cross-section of a 3µm thick GaN film grown on a 20 nm thin GaN buffer layer on top of a sapphire substrate (top). Cross sectional TEM of a laterally overgrown GaN layer on a SiO_2 mask and window area (bottom)……………………………….. 7

4. Comparison of GaN/AlGaN based HFET planar structure (top), and self-aligned implanted structure (bottom) showing selective area doping under the metal contacts……………………………. 12

5. Possible results from ion impact with the surface of a material illustrating sputtering, implantation, substrate damage, ion recoil and creation of secondary electrons…………………… 14

6. Interaction of an incident ion on a crystal lattice. Both the incoming ion and lattice atoms are deflected in nuclear elastic collisions, while electronic inelastic interactions contribute to energy loss but not appreciable angular deflections (top). Rate of energy loss dE/dx versus $(energy)^{1/2}$, showing nuclear and electronic loss contributions (bottom)…………………………………………………….. 17

7. Schematic of the disorder produced along the individual paths of light and heavy ions showing the damage created by a heavy ion as uniform through the ion path, while the damage of the light ion is sporadic and concentrated at the end of the ion path………….. 19

8. Atomic force microscope (AFM) images of GaN after annealing at 1100 ^{o}C for 15 seconds, uncapped (top) or capped with reactively sputtered AlN (bottom), which was subsequently removed in selective KOH solution. For both Images the vertical scale is 50 nm/division while the horizontal scale is 2 μm/division………………………………………….. 23

9. Reverse current-voltage (I-V) characteristics for Pt/Au contacts on GaN annealed at 1100°C, 15 s either uncapped (B1) or capped with AlN (B2). This is showing initially semi-insulating GaN implanted with ^{28}Si (100 keV, 5x10^{13} cm^{-2}) to simulate a MESFET channel implant…………………………………… 24

10. Energy band diagram showing additional leakage current caused by tunneling from defect states in addition to the current by thermionic emission……………………………………..………….. 32

11. I-V characteristics from n-GaN diodes before and after H_2 (top) and N_2 (bottom) plasma exposure (150 W rf chuck power, 5 mTorr) at different ICP powers……………………………………………………. 33

12. I-V characteristics from p-GaN samples exposed to either H_2 (top) or Ar (bottom) ICP plasma discharges (150 W rf chuck power) as a function of source power prior to deposition of the Schottky contact………………………………………………………… 34

13. Forward turn-on voltage of p-GaN diodes exposed to ICP Ar plasma discharges (150 W rf chuck power) at different ICP source powers prior to deposition of the Schottky contact……………….. 36

14. Breakdown voltage as a function of depth removed in a 0.1 M NaOH wet-etch solution for p-GaN diodes (top). Breakdown voltage as a function of thermal annealing temperature for p-GaN diodes (bottom)……………………………………………………. 37

15. Schematic of p-type planar Schottky diode structure (top), or n-type planar Schottky diode structure (bottom)………………………. 39

16. I-V characteristics from n-GaN diodes before and after Ar plasma damage and subsequent N_2 plasma exposure at different temperatures…………………………………………………….... 41

17. I-V characteristics from n-GaN diodes comparing N_2 plasma exposure and annealing at the same temperatures………………………… 42

18. I-V characteristics from n-GaN diodes before and after Ar plasma damage and subsequent N_2 plasma exposure at 350°C and different pressures………………………………………………... 43

19. N-GaN diodes showing plot of V_B versus treatment temperature for N_2 plasma exposure or annealing………………………… 44

20. AFM scans of n-GaN surface before and after Ar plasma damage and after subsequent N_2 plasma treatment……………….. 45

21. I-V characteristics from p-GaN diodes before and after Ar plasma damage and subsequent N_2 plasma exposure at different temperatures…………………………………………………... 47

22. I-V characteristics from p-GaN diodes comparing N_2 plasma exposure and annealing at the same temperatures………………………… 48

23. I-V characteristics from p-GaN diodes before and after Ar plasma damage and subsequent N_2 plasma exposure at 350°C and different pressures……………………………………………... 59

24. P-GaN diodes showing plot of V_B versus treatment temperature for N_2 plasma exposure or annealing………………………… 50

25. Simulated Be implant ion profile in GaN with multiple-energy O co-implants………………………………………………………………… 52

26. Simulated Mg implant ion profile in GaN with multiple-energy O co-implants…………………………………………………….…………… 53

27. Sheet resistance as a function of anneal temperature in Be + O co-implanted GaN………………………………………………… 56

28. Mobility as a function of anneal temperature in Be + O co-implanted GaN………………………………………………………. 57

29. Sheet carrier concentration as a function of anneal temperature in Be + O co-implanted GaN…………………………………………… 58

30. Sheet carrier concentration as a function of anneal temperature in Be + O co-implanted GaN in Arrhenius form…………………….……….. 59

31. Sheet carrier concentration as a function of anneal temperature in Mg + O co-implanted GaN……………………………………………... 61

32. Mobility as a function of anneal temperature in Mg + O co-implanted GaN…………………………………………………………. 62

Abstract of Thesis Presented to the Graduate School
of the University of Florida in Partial Fulfillment of the
Requirements for the Degree of Master of Science

CO-IMPLANTATION AND DRY-ETCH DAMAGE RECOVERY BY PLASMA NITRIDATION IN GaN

By

Donald G. Kent III

August, 1999

Chairman: Stephen J. Pearton
Major Department: Materials Science and Engineering

In order to produce effective GaN based electronic devices such as thyristors, P-I-N diodes, and HBTs it is necessary to produce active regions with p-type doping. To date, Mg has been found the most effective impurity that results in p-type conducting GaN. However, the activation energy of Mg doped GaN is relatively high (150-200 meV). The atomic concentrations needed to obtain effective hole densities (>10^{17} cm^{-3}) at room temperature are in the range of 10^{19}-10^{20} cm^{-3}.

One method to increase the hole density is by molecular co-doping. It has been shown that by co-doping with donors and acceptors it is possible to increase the solubility limit of both impurities beyond the limit of either impurity. The first aspect of this research focuses on achieving p-type conductivity in GaN through selective co-doping via ion implantation.

Beryllium and magnesium were co-implanted with oxygen into GaN at precise donor-to-acceptor ratios of 0.5-2. High activation efficiency was achieved for Be + O co-implants at a donor-acceptor ratio of 2 and anneal temperatures of 1050-1100°C. The

activation process was not a simple, single-step mechanism. Hall data indicated a relatively low (≤ 100 meV) ionization energy for Be in the co-implanted samples. This process may have application in improving p-ohmic contact resistance by selective area Be + O implantation. By sharp contrast Mg + O co-implants produced n-type conductivity under all conditions.

Due to the unique material properties of GaN such as its wide bandgap, high thermal conductivity, and large breakdown field; it is becoming the material of choice for many optoelectronic, high power, and high temperature devices. Dry-etching has become the dominant patterning technique for this material system. It produces high etch rates, anisotropy, and smooth sidewalls. The second aspect of this research focuses on recovering dry etch damage in GaN through plasma nitrogen treatments.

Exposure of dry-etch damaged p- and n- GaN to N_2 plasmas at elevated temperatures (175-350°C) is found to produce partial recovery of the electrical properties of the near-surface region. The recovery is due to two mechanisms —an annealing effect and a nitridation of the initially N_2 deficient surface. A degree of surface smoothing was also obtained with N_2 plasma exposure. The extent of the damage recovery however is less than complete for both conductivity types of GaN.

CHAPTER 1
INTRODUCTION

1.1 GaN Applications

GaN and related III-Nitride material systems (Indium and Aluminum) are quickly becoming the third most important commercial semiconductor after silicon and conventional III-V compounds based on GaAs. The Unique combination of GaN's direct bandgap (3.4 eV) and bandgap engineering allow the production of a wide range of photonic devices. This is due to the fact that GaN forms ternary alloys with In or Al and results in light emitters –both lasers and light emitting diodes— with a range from the red for InN (1.89 eV bandgap) to the deep UV for AlN (6.2 eV bandgap).

The mid to late 1990s have seen an explosive growth in the Gallium Nitride device market as shown in Figure 1 (top). Optoelectronics have been leading the way with the production of blue, green and white LEDs and laser diodes. These devices have found practical application in many areas including full-color outdoor signs, traffic lights, automotive interior lighting, general-purpose indicator/display applications, sensing, spectroscopy, and next-generation optical storage systems. These advances were triggered by the development of p-type doping in 1989 by Amano et al.[1], which was rapidly followed by the fabrication of p/n junctions, light emitting diodes, and laser

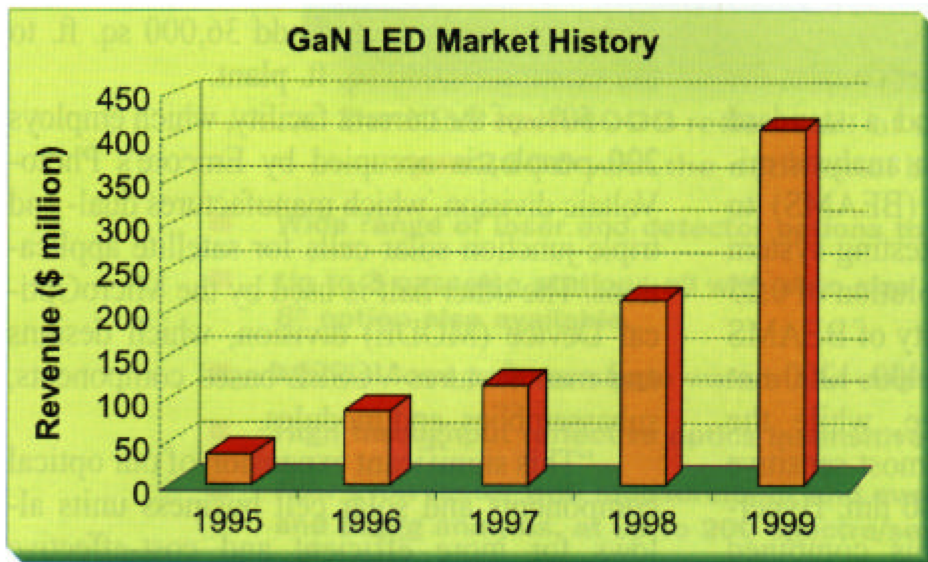

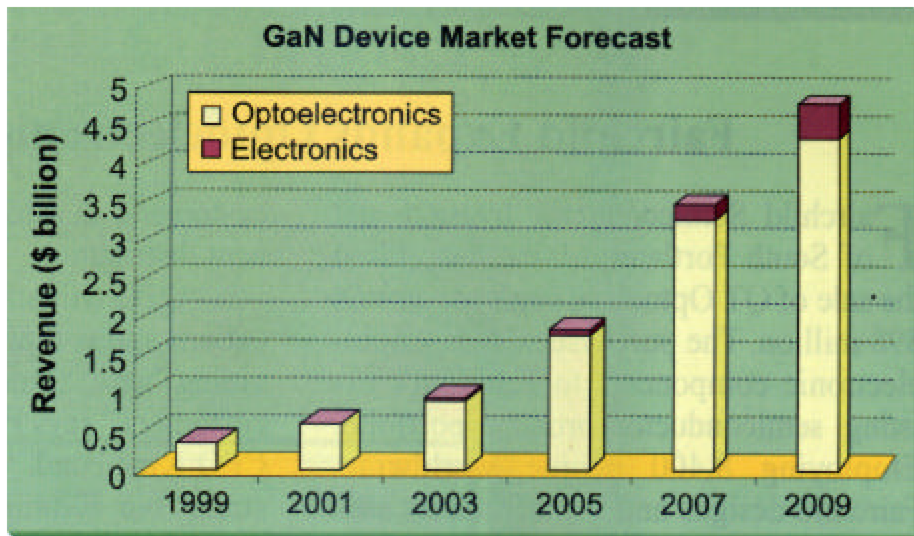

Figure 1 GaN LED market history (top). Market forecast for GaN based optoelectronic and electronic devices (bottom).[2]

structures. Advances in crystal growth techniques have given these devices commercial viability via longer lifetimes by decreasing the density of native defects present in this material. The renaissance of advancements in GaN based LEDs is illustrated in Figure 2 which shows a chronological plot of the evolution of the energy conversion efficiency of GaN and GaAs LEDs.[3]

In addition to optical applications, III-Nitride heterostructures are very promising candidates for demanding transistor applications such as high power, high frequency microwave amplifiers and switches.[4-8] The physical properties that makes them ideal for these applications are their wide bandgap and high breakdown fields. As can be seen in the bottom of Figure 1, the electronic device market is a small portion of the overall GaN market, and in fact electronic devices based on GaN are not expected to hit commercial markets until 2002.[2] There are several material problems that need to be overcome to insure the position of electronic based GaN devices and include: substrates with a low density of crystal defects; low R_c n-ohmic contacts (the requirements are harsher than for photonic devices, with $R_c \leq 10^{-7}$Ocm^{-2} being the aim); stable and reproducible Schottky contacts, and low damage dry etching that maintains surface stoichometry.[9]

1.2 GaN Material Issues

1.2.1 Growth Defects

There have been several materials issues with GaN that to date have prevented the fabrication of devices with low defect densities. Commercial LEDs operate with

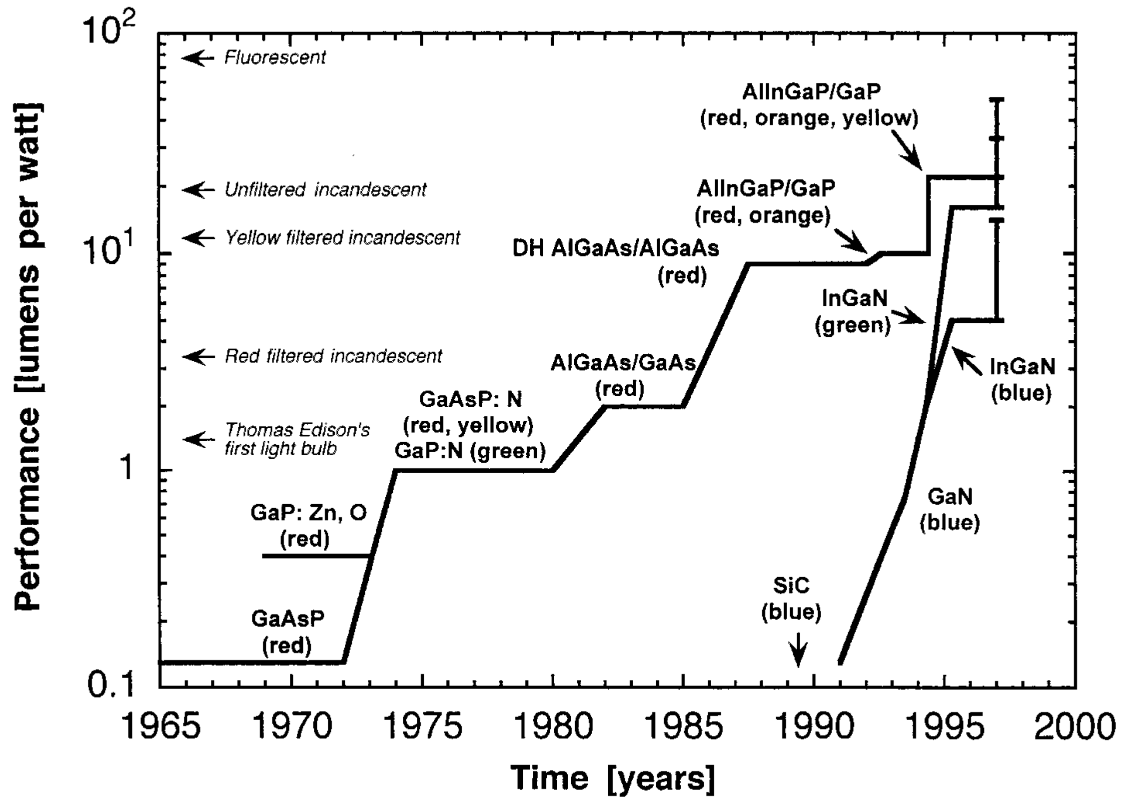

Figure 2 Chronological representation of the development of the performance of GaN- and GaAs-based light emitting diodes.[3]

threading dislocations on the order of 10^8 cm^{-2}, sometimes even reaching 10^{10} cm^{-2}.[10] The root cause of this high number of defects has to do with the high bond strength of GaN (8.92 eV/atom) and resulting high melting point near 2800°C. In this temperature range the equilibrium partial pressure of nitrogen is extrapolated to be above 45 kbar which has prevented any single crystal growth from the melt.[11-12]

GaN has only been able to be obtained through heteroepitaxial methods on lattice-mismatched substrates such as SiC or sapphire. The differences in lattice parameter and thermal expansion coefficients of these materials creates misfit stress relaxation during growth and additional stresses upon cooling down, which contributes to the large density of threading dislocations and stacking faults. These defects originate with the island nucleation on the highly lattice mismatched substrate, and continues as the islands coalesce to the film and end up being propagated through the main layer. Table 1 shows a comparison of lattice parameter and thermal expansion coefficient for the two

Material	57. Lattice **Parameter a (Å)**	Latt ice **Mismatch To**	**Thermal Expansion Coefficient (at 300K) (10^{-6} K^{-1})**
w-GaN	3.189		5.59
Al_2O_3	4.758	-14%	7.5
6H-SiC	3.08	+4%	4.2

Table 1 Comparison of sapphire and SiC: the two most popular substrate materials for heteroepitaxal growth of GaN, showing lattice parameter and thermal expansion coefficient comparisons.

most popular GaN substrates. It is seen that sapphire has a ~14% lattice mismatch while SiC has a ~4% mismatch.

The advances in the late 1980s and 1990s in crystal growth techniques – particularly buffer layer growth and lateral epitaxial overgrowth [13,14]— has not only paved the way for optoelectronics based on GaN, but has also given device designers the lower defect starting material that is needed to fabricate electronic devices. The growth of AlN buffer layers was employed in 1986 by Amano et al.[13] and they greatly improved the structural and electrical quality of the resulting GaN as shown in the TEM image at the top of Figure 3. This buffer layer reduces the strain and hence the defect density, however these defect levels can still be high with values in the 10^9 cm^{-2} range.

The lateral epitaxial overgrowth technique takes advantage of the large anisotropy of the GaN growth rate in the [0001] direction compared with the lateral growth. Due to this anisotropy it is possible to grow high-quality layers on a patterned template as shown in the bottom of Figure 3. After first growing a GaN layer, a pattern is formed lithographically out of SiO_2 with 'windows' to the GaN layer. Process conditions are adjusted so that further growth of GaN proceeds only through the openings in the mask. As soon as the GaN thickness is greater than the mask thickness, horizontal overgrowth becomes dominant. By successive treatments of this technique the density of threading dislocations has been reported to be as low as 10^6 cm^{-2}.[15] This technique is one of the key steps in providing high-quality material for long-lived devices and electronic applications.

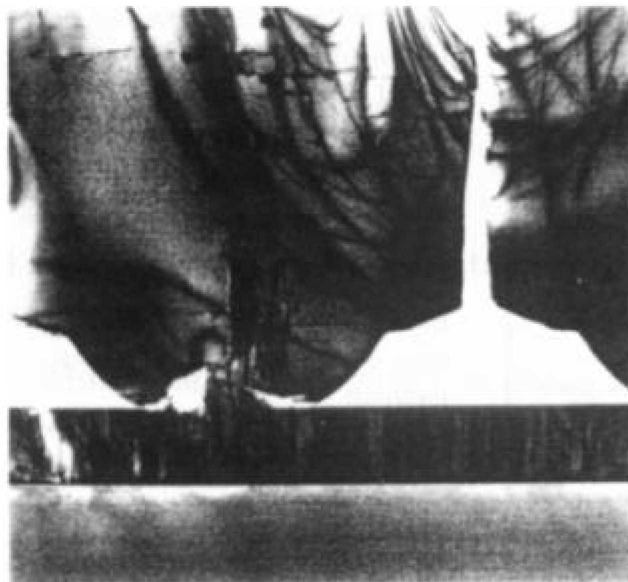

Figure 3 TEM cross section of a 3μm thick GaN film grown on a 20 nm thin GaN buffer layer on top of a sapphire substrate (top).[15] Cross sectional TEM of a laterally overgrown GaN layer on a SiO_2 mask and window area (bottom).[15]

1.2.2 Defects and Doping

Viable GaN semiconductor technologies could not be developed in the 1970s and 1980s mainly due to the lack of p-type conducting material. During these years while the industry was maturing all of the GaN produced had an unintentional high n-type background, which was attributed to impurities or native defects that introduce shallow donor levels. Most of the research on defects in GaN has focused on point defects such as cation/anion vacancies, antisites, interstitials, substitutional impurities, and complexes of these defects. The ever-present growth defects such as dislocations, twins, and stacking faults are expected to effect doping, however few studies on the nature of their influence on electrical and optical properties have been conducted.

The activation energy of unintentionally doped GaN is in the range of 30-40 meV.[17-19] It is generally accepted that nitrogen vacancies (N_v) are responsible for this shallow hydrogen-like donor level.[20,21] The Gallium vacancy is predicted to be a shallow acceptor and has been found to produce an acceptor level 0.3 eV above the valence band edge.[22] All other native defects are predicted to form levels deeper in the bandgap. Most of these have high activation energies and are not expected to occur in large concentrations at room temperature.

The polar nature of the Ga—N bond (~39% ionic) is one of the causes of complexity encountered when trying to impurity dope this material. Impurities do not form shallow levels in the band gap of ionic solids because the electrons are more tightly bound to the ionic cores, however because GaN has mixed polar-covalent bonds several n-type impurities have been found that form shallow donor levels. Table 2 illustrates the shallow acceptor and donor energy levels in GaN.[23]

Table 2 Shallow acceptor and donor levels in GaN.

Defect or Impurity	Type	Energy in meV (method of measurement)
N-vacancy	Donor	
O	Donor	32-37 (Hall), 78 (Hall)
Si	Donor	12-17 (Hall), 27 (Hall), 22 (PL)
Mg	Acceptor	~165 (Hall)
Be	Acceptor	250 (PL), 90-100 (PL) by MBE
Ca	Acceptor	169 (Hall)

The attainment of p-type doping in GaN was achieved accidentally in 1989 by Amano et al. while applying low-energy electron beam irradiation in an SEM to Mg doped MOCVD grown GaN.[1] It was realized that the energy from the e-beam disassociated the hydrogen from the Mg -H complex that was passivating the Mg acceptors.[24-27] It was later discovered that a simple post-growth heat treatment of MOCVD grown p-doped layers activated the Mg acceptors.[28] Presently, p-type doping by magnesium is routinely achieved, and when grown by MBE no post-growth heat treatment is necessary because there is no hydrogen present to passivate the acceptors.

To date Mg has been the most effective acceptor for obtaining p-GaN with the lowest activation energy, however this acceptor ionization energy is still several kT above room temperature with reported ranges between 150-180 meV.[29,30] Due to this high activation energy, at room temperature only ~1 percent of the acceptors are ionized and producing holes. This means that in order to obtain effective hole densities the Mg

doping needs to be two orders of magnitude greater than the hole concentration. Recently, MBE grown GaN lightly doped with Be has been produced with a lower than previously reported activation energy of 90-100 meV.[132] However, as the Be incorporation was increased the samples showed no evidence of photoluminescence.

Another source of unintentional n-type conductivity is donor impurities, particularly the group VI impurity oxygen. Currently it is well known that oxygen creates a shallow donor level in GaN and at high concentrations it forms an impurity band that can merge with the conduction band.[20,31-34] Due to contamination, it is suspected of being incorporated during growth. Oxygen impurity and nitrogen vacancy theories are currently considered to be the cause of the auto-doping of GaN and the resulting high n-type background.

CHAPTER 2
BACKGROUND INFORMATION

2.1 Ion Implantation

2.1.1 Introduction

In order to fabricate active regions in a semiconductor, conducting regions or layers must be created. The choice to use ion implantation, diffusion, or epitaxial methods for creating these active regions is based upon the design of the device's final electrical characteristics and the process sequence. Ion implantation is the choice for

many process applications.[35-38] This is principally due to the fact that doping by ion implantation is relatively low cost; provides good control of dopant concentration; and the depth and implant profile is highly reproducible (a factor that is critical for the semiconductor process industries).

One good example of how ion implantation can affect III-Nitride devices is illustrated in Figure 4 [39]. This figure shows two separate structures that are used to create the same AlGaN/GaN high electron mobility transistor (HEMT). Currently most of these structures are fabricated in the planar structure as illustrated at the top of Figure 4. In this structure the ohmic source and drain contacts are placed directly on the wider bandgap AlGaN layer. One disadvantage of this method occurs because there is no local region of high doping underneath the metal contact thereby increasing the contact

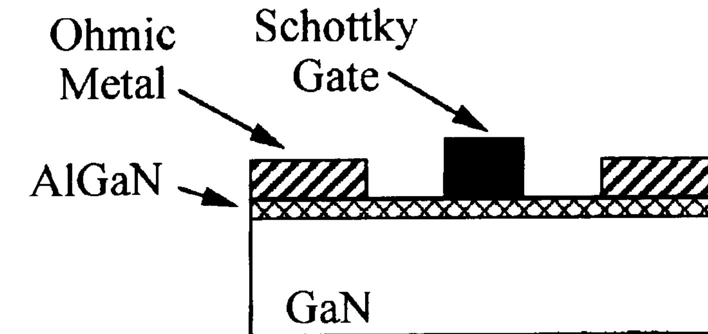

Planar Structure

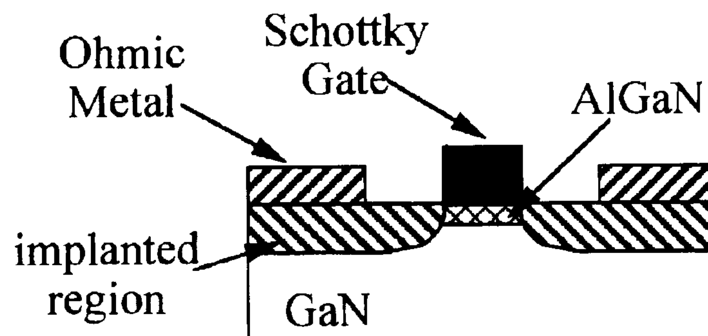

Self-aligned Implanted Structure

Figure 4 Comparison of GaN/AlGaN based HFET planar structure (top), and self-aligned implanted structure (bottom) showing selective area doping under the metal contacts.

resistance between the AlGaN and metal ohmic contacts. This higher contact resistance may produce diminished performance of the device by reducing its gain and current carrying capabilities.[40]

Ion implantation is the process of introducing impurity atoms to the semiconductor by: ionizing the impurity element; accelerating it through a high potential (from kV to higher than MV energies); and then directing this beam of ionized particles into the semiconductor substrate. The ions, after colliding with the substrate lose energy in collisions with the lattice atoms and after some distance come to rest in the semiconductor. High-dose ion implantation is used to make highly conductive n+ or p+ layers and allows the formation of low resistivity ohmic contacts.[41] Ion implantation can also be used to selectively dope regions within devices or for implant isolation between active areas.

2.1.2 Ion Interactions

When energetic ions strike a surface there are several effects that can occur as illustrated in Figure 5. Ions with low energy may simply bounce off the target, while at energies up to about 10 eV the ion can also adsorb to the surface. At ion energies starting around 10 keV the ion penetrates into the material many atomic layers losing energy along the path through several mechanisms.[42] It is at these higher energy levels that ion implanters operate.

As high-energy ions enter a semiconductor –considered as charged ions with a cloud of screening electrons for the purpose of determining range effects— they begin to

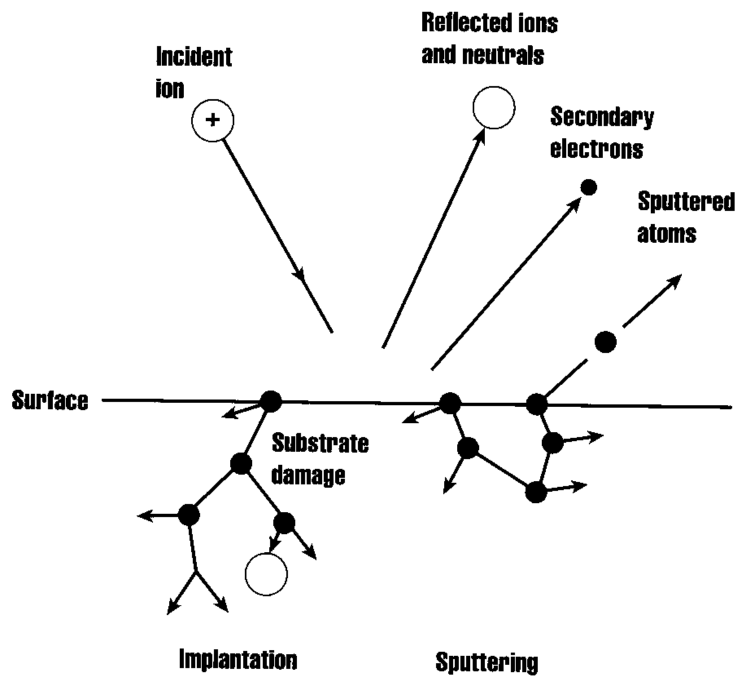

Figure 5 Possible results from ion impact with the surface of a material illustrating sputtering, implantation, substrate damage, ion recoil and creation of secondary electrons.

lose energy. The first energy loss mechanism that ions experience is through interaction with the "sea" of both valence and core electrons of the target atom. Much of the lattice space is composed of this cloud of electrons and many of these interactions will occur. Even if the electron is not in the path of the ion it will lose energy through electron-ion coulombic interactions. Due to the large number of these interactions the sea of electrons can be modeled as a continuum, and the effect of the ion passing through this electronic continuum is similar to that of a particle moving through a fluid. The energy loss mechanism is similar to a viscous loss in a fluid and is proportional to the velocity of the ion. This viscous drag force can be expressed by the following relation:

$$F_D \propto v \propto \sqrt{E} \tag{2.1}$$

The electronic stopping is usually expressed as an energy gradient or loss per unit length of the traveled path, and given the symbol S_e and where k_e is a proportionality constant that depends on the ion and target species.

$$S_e = \frac{dE}{dx}\Big|_e = k_e\sqrt{E} \tag{2.2}$$

The second type of energy loss mechanism of ions implanted in a material is through nuclear collisions. Ions implanted under normal process conditions come to rest in a material up to several thousand angstroms deep. This is on the order of the number of elastic collisions the ion will undergo (since atomic spacing is on the order of angstroms). Because there are a discrete number of these nuclear collisions between the ion and atom core the energy loss mechanism cannot be modeled as if it were a continuum. Any single nuclear collision will depend upon the previous collision and similarly all the way back to the first collision upon entering the target.

Nuclear collisions can involve large discrete energy losses and are capable of producing large angular deflections of the incoming ion as shown in Figure 6 (top). These collisions are responsible for the production of lattice damage and the subsequent displacement of substrate lattice atoms. Electronic collisions on the other hand produce small energy losses on a per collision basis and produce negligible deflection of the incoming ion. Figure 6 (bottom) shows the relative importance of these two energy loss mechanisms as a function of ion energy. At low ion energies energy losses through nuclear collisions dominate while at higher energies, energy losses through electronic collisions dominate. The average energy loss will also be a function of the ratio of the mass of the ion to that of the substrate atom. The smaller this ratio the larger the average energy loss will be.

Since the ions are uniformly distributed across the surface of the wafer, a statistical distribution of depths can be used to describe the profile of the implanted ions. To first order approximation a gaussian distribution can be used to model the range of depths of ions in an amorphous solid by:

$$N(x) = \frac{\Phi}{\sqrt{2\mathbf{p}\Delta R_p}} e^{-(x-R_p)^2/2\Delta R_p^2} \qquad (2.3)$$

The projected range is given by R_p; the standard deviation (straggle) of the projected range by ?R_p; and the dose by F. Due to the statistical nature of the scattering events the ions will be deflected laterally as well as vertically and thus the profile will also have a lateral standard deviation (lateral straggle) ?Rp $\perp$.

Additional moments can be added to the gaussian profile to more accurately

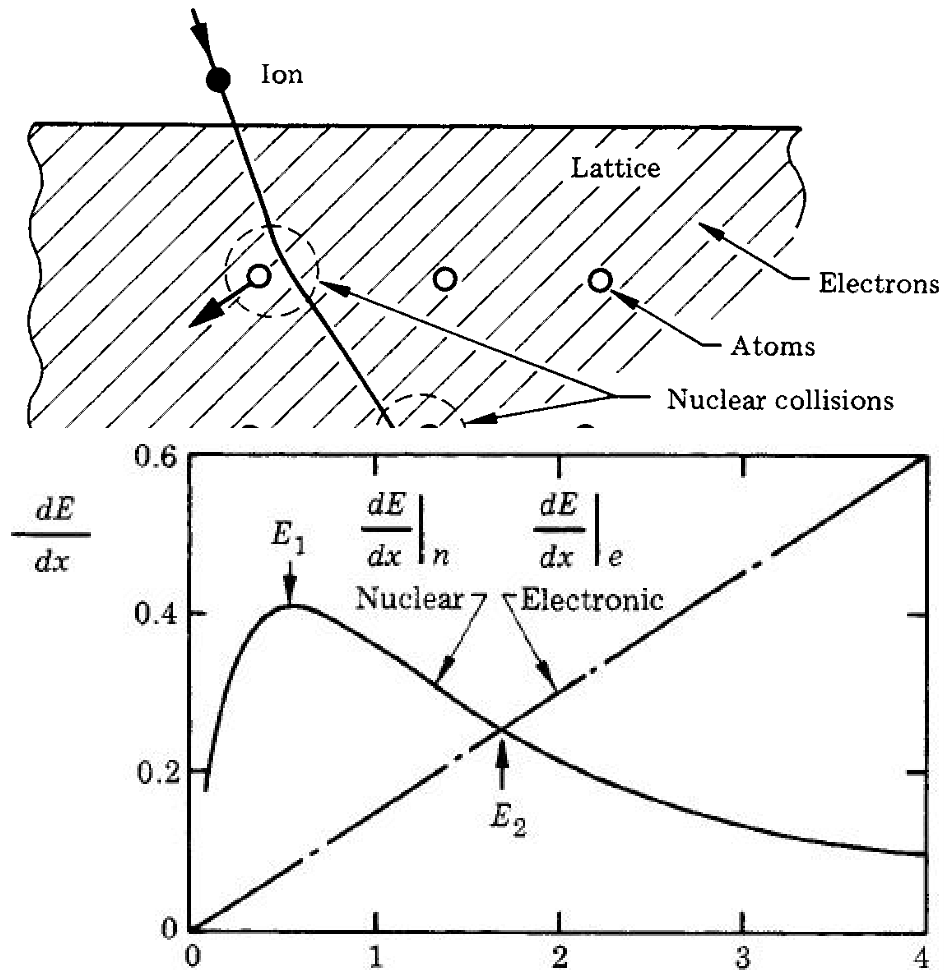

describe the profile for lower concentrations. When implants are performed in single crystal substrates an effect called channeling can occur that may greatly distort the predicted final position of the ion. If the incoming ion is parallel to a major crystal orientation it could then travel long distances with relatively little energy loss through glancing elastic collisions. This channeling can add a large "tail" to the end of the original gaussian distribution. To offset this problem and minimize the channeling effect implants can be rotated and tilted and are most often performed off axis with a typical tilt angle of 7°. Another method to prevent channeling is to destroy the lattice by preamorphizing the substrate by bombardment with high doses of ions prior to the dopant

Figure 6 Interaction of an incident ion on a crystal lattice. Both the incoming ion and lattice atoms are deflected in nuclear elastic collisions, while electronic inelastic interactions contribute to energy loss but not appreciable angular deflections (top). Rate of energy loss dE/dx versus $(\text{energy})^{1/2}$, showing nuclear and electronic loss contributions (bottom).

implantation. This technique works well for silicon,[43] however it is not an effective method for III-V semiconductors due to poor recrystallization, which leads to higher levels of residual disorder.

2.1.3 Implantation Damage

One drawback of ion implantation is the damage created during energetic ion bombardment. When incoming ions collide with lattice atom cores these atoms can be displaced and gain enough energy to displace other atoms creating a collision cascade. Implantation creates considerable lattice damage in the form of vacancies, interstitial

atoms, amorphous regions and other defects that must be repaired. Also, for the implanted species to act as a dopant it must come to rest on a lattice site or be "activated". Both damage repair and activation are usually done under the same annealing step. As shown in Figure 7, a light ion such as boron in Si loses energy primarily in electronic collisions and only has occasional large energy transfer collisions,

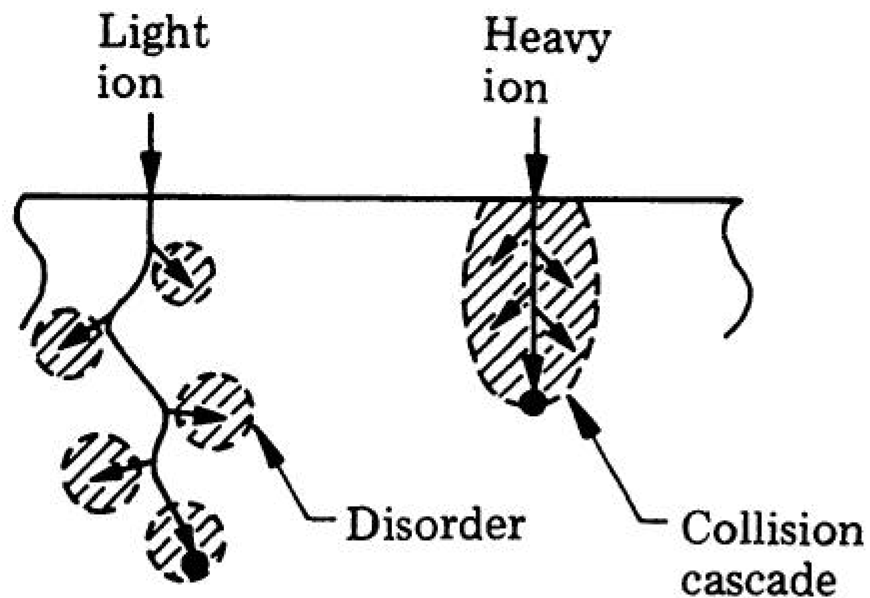

Figure 7 Schematic of the disorder produced along the individual paths of light and heavy ions showing the damage created by a heavy ion as uniform through the ion path, while the damage of the light ion is sporadic and concentrated at the end of the ion path.

which mostly occur at the end of its path. However a heavy ion such as Sb loses energy primarily in nuclear collisions and produces a dense cascade of collisions and disorder along the entire ion path.

As an ion passes through the crystal, point defects consisting of interstitials and vacancies or Frenkel pairs are generated, however more complex defects can be created such as di- or trivacancies along with clusters of these defects. Depending upon the ion, the dose, and the implant temperature; the implant damage can consist of either amorphous layers or extended crystalline defects such as dislocations and stacking faults. Extended defects can be caused by an accumulation of point defects and are common in implanted materials. During implantation each ion produces a region of disorder along the ion path. The amount of lattice disorder builds up until an amorphous region forms. The dose required to form a uniform amorphous region is termed the critical dose (F_c). It has been found that the amorphization dose for 100 keV Si-implantation in GaN at room temperature is ~$2x10^{16}$ cm^{-2}.[44,45]

The electrical nature of implanted dopant ions is determined by the behavior of the damaged regions. These ion damaged regions produce a high resistivity layer that contains electron and hole traps and recombination centers that reduces the carrier mobility and is the basis of damage-induced implant isolation effects that are in use in III-V semiconductors. The objective with few exceptions however is to produce a layer with a controlled number of electrically active dopants. To accomplish this the implanted ion must occupy a substitutional lattice site and the concentration of electrically degrading effects should be much less than the concentration of the dopants. Otherwise the defects may compensate the electrical activity of the dopant. Residual damage in

GaN – in particular the nitrogen vacancy— has been shown to create a shallow donor level and is thought to be responsible in part for the high n-type background found in GaN.[46-52]

Post implant annealing is required to repair the disorder and activate the implanted ions by causing them to diffuse to a lattice position and hence become electrically active. For III-V semiconductors the annealing temperature required to diffuse the dopant to the lattice site is greater than the temperature at which the surface of the semiconductor degrades through the preferential loss of the type V element (nitrogen). In previous Si implantation studies of GaN it has been shown that significant implantation induced damage remains even after an 1100°C activation anneal that produces electrically active donors.[53] A temperature well above 1100°C is needed to remove the implantation induced damage, however since GaN decomposes at these temperatures certain precautions must be taken to protect the surface from degradation.

For GaN there are several methods commonly used to protect the surface during annealing. The first method is capless proximity annealing in which two similar wafers are placed face to face with each other in order to minimize the loss of nitrogen by supplying a simple overpressure of nitrogen. This method is the most popular for research, however it does have several disadvantages such as cross contamination, mechanical damage, and loss of nitrogen due to edge effects.

The second method for device fabrication or higher temperature anneals is to encapsulate the GaN in a dielectric such as AlN. Since AlN has a higher bond strength than GaN it acts to suppress the dissociation of the GaN.[54] The AlN cap can be

deposited by using an argon plasma to sputter an Al target in flowing N_2. Following annealing, the AlN is removed in a selective KOH-based etch at 60-70^oC.[55]. This etch has been shown to remove the AlN at rates between 60-10,000 Å/min, dependent upon the film quality. No measurable etching of GaN is observed under these conditions.[56] Figure 8 shows three-dimensional atomic force microscope (AFM) images of the surface of uncapped (top) and AlN capped (bottom) GaN samples after annealing at 1100^oC. The sample without the cap has become markedly rougher than the AlN capped sample, which is attributed to more nitrogen loss than the capped sample. Likewise the electrical properties of Schottky diodes show a 3-4 order of magnitude degradation of reverse breakdown characteristics for uncapped GaN as compared to AlN capped GaN, as shown in Figure 9.[54]

The last method to protect the GaN semiconductor surface that has been extensively studied is the use of a nitrogen overpressure. This method is also very popular for other III-V semiconductors. One way to achieve this is to supply a reservoir of excess semiconductor material in the form of a powder or finely crushed material.[57] This excess material will release nitrogen due to its large surface area, which will provide the overpressure to the active wafer surface. Success has been reported in using InN, GaN and AlN powders as the material in the reservoir. In this technique N-loss from the GaN occurs at $\leq 1050^oC$.[58]

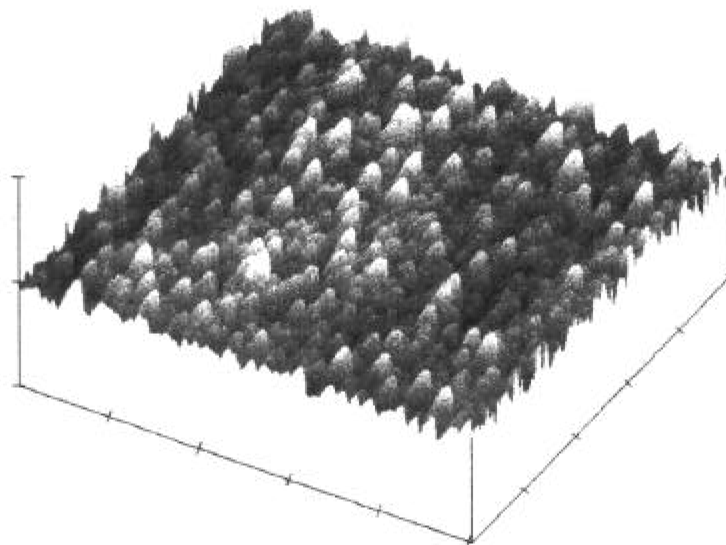

(a) RMS = 4.02 nm

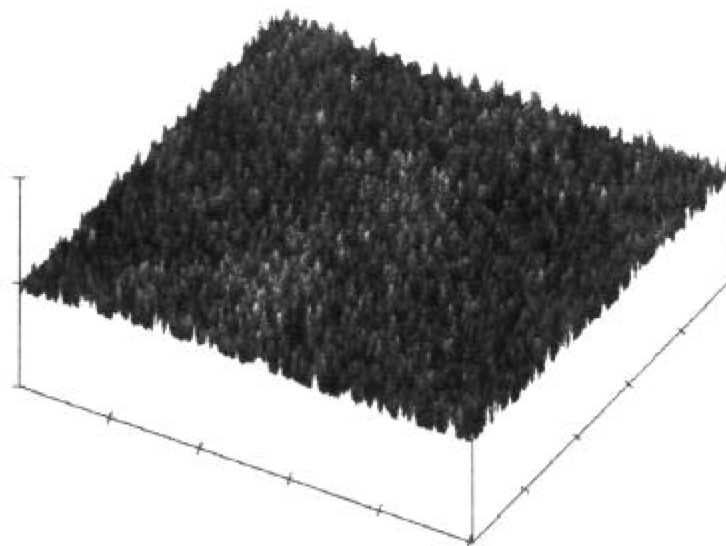

(b) RMS = 2.51 nm

Figure 8 Atomic force microscope (AFM) images of GaN after annealing at 1100°C for 15 seconds, uncapped (top) or capped with reactively sputtered AlN (bottom), which was subsequently removed in selective KOH solution. For both Images the vertical scale is 50 nm/division while the horizontal scale is 2 µm/division.

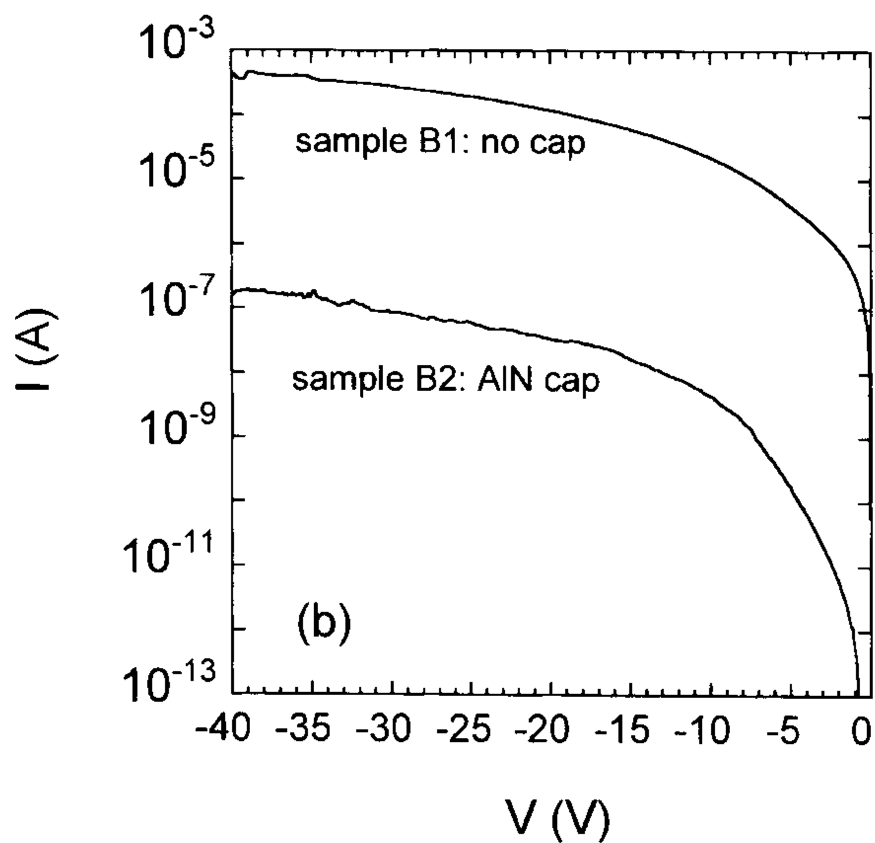

Figure 9 Reverse current-voltage (I-V) characteristics for Pt/Au contacts on GaN annealed at 1100°C, 15 s either uncapped (B1) or capped with AlN (B2). This is showing initially semi-insulating GaN implanted with ^{28}Si (100 keV, $5x10^{13}$ cm^{-2}) to simulate a MESFET channel implant.[19]

2.1.4 Co-Implantation

The specific contact resistance of p-ohmic contacts on GaN devices such as heterojunction bipolar transistors, lasers and p-i-n photodetectors is often a limiting factor in the reliability and speed performance of these structures.[9] The large ionization energies of acceptor dopants in GaN leads to relatively low hole densities ($\leq 10^{17}$ cm^{-3}) at room temperature, even when the acceptor concentration is ~10^{19} cm^{-3}.[59,60] Moreover, attempts to introduce higher acceptor concentrations often lead to type-conversion through the creation of interstitial defects with donor nature.[60] One of the methods for circumventing this problem is to grow Mg-doped AlGaN/GaN superlattice structures in which spontaneous and piezoelectric polarization effects enhance the hole concentration.[61-75] In these structures the acceptor ionization energy is significantly reduced relative to bulk GaN.[75] Similar results are reported with Mg-doped InGaN/GaN superlattices.[76,77]

To create local regions with higher hole concentrations means either that selective regrowth of these superlattices must be performed, or that methods for achieving higher implant activation efficiencies for acceptors be developed. Ion implantation of p-dopants in GaN (Mg or Ca) can produce relatively good activation efficiencies at moderate doses (~10^{14} cm^{-2}) if the acceptors are annealed under conditions that maximize the substitutional fraction and which remove compensating, damage-related donor states.[78-87] However the resulting sheet resistances are well above those necessary to achieve acceptably low p-ohmic contact properties. One concept that might improve this

situation is that of co-doping with acceptors and donors to prevent self-compensation.[88,89]

It was shown by Reiss et al.[90] that co-doping with acceptors and donors increases the solubility of both impurities beyond the solubility limit of either impurity in the given semiconductor. He demonstrated this phenomenon by using Li as the donor and Ga the acceptor in Germanium. One of the advantages of this ion pairing (beyond higher solubility) is increased carrier mobility. This higher mobility is predicted due to the fact that ion pairs possess dipolar fields and consequently have scattering cross-sections that are much smaller than those of point charges (which are long-range coulomb scatterers).

More recently Brandt et al.[91] doped GaN with Be and O by MBE and showed that this molecular co-doping greatly enhanced the mobility of holes in p-GaN, which he attributed to the short range dipole scattering effect of the spatially correlated ion pairs. In particular, there is a theoretical prediction that the highest hole concentration will occur at the donor/acceptor ratio of 1|2.[88,89] With this research we report experiments on implantation of Be + O and Mg + O into GaN, at controlled ratios of donor-to-acceptor ranging from 0.5-2.0. Beryllium is an attractive choice for these experiments because of the low implant damage it creates in GaN[92,93] and the theoretical evidence that it has a shallow acceptor level in wurtzite GaN.[94]

2.2 Dry Etching of GaN

2.2.1 Introduction

Plasma etching has become the preferred method of patterning III-Nitride materials because of its ability to produce smooth surfaces and anisotropic features.[9,95-102] In the past plasma etching has been applied to the processing of III-V photonic devices such as LEDs and laser diodes where the main requirements have been for high etch rates, anisotropic profiles, smooth sidewalls and equi-rate etching of dissimilar layers. However, as the interest in high power, high temperature electronic devices has increased so have the requirements placed on plasma etching. Because of the shallower etch depths and decrease in critical dimensions of these devices; the dry etch requirements now include smooth surface morphology and low plasma induced damage. These requirements are hampered by the fact that GaN (and other III-Nitrides) etch at a much slower rate with chlorine-based plasmas in contrast to traditional III-V compounds. This is generally attributed to the bond strength of GaN as compared to GaAs, 8.92 eV/atom and 6.52 eV/atom respectively.[103]

Since GaN has relatively high bond strength, effective dry etching occurs under conditions of high ion flux or high ion energy.[95,96] This can produce a damaged surface region, whose main electrical signature is an increase in n-type conductivity.[98] If one starts with n-GaN, dry etch damage leads to higher near surface conductivity. Conversely, the surface of initially p-GaN experiences a decrease in p-type conductivity and in cases of high ion flux or energy can be converted to n-type material through

compensation by shallow donor levels as a result of etching.[104-110] The depth of the damaged region is typically 400-600Å for Inductively Coupled Plasma (ICP) etching at moderate powers for the range used in device processing.

Several different methods for removing the damage have been reported, including thermal annealing, sequential oxidation/chemical stripping, and finally dissolution in hot base solutions.[95,96,110-112] There have also been recent reports on use of elevated temperature N_2 plasma treatments for reducing the effects of plasma damage in n-GaN.[113] While contact resistance was used as one measure of damage recovery, most of the past work has focused on surface morphology or luminescence changes. This work focuses on using N_2 plasma treatments to recover dry-etch damage. This effect is characterized by looking at the reverse breakdown voltage (V_B) of n- and p-GaN Schottky diodes, which is a sensitive indicator of this damaged state.

2.2.2 Plasma Etching

Plasma etching of GaN has been developed, in part due to the poor effectiveness of wet etching techniques. Immersion of GaN in strong acid or base solutions at elevated temperatures (150-300°C) can produce etching in certain crystallographic directions, but this has limited applications for high production pattern transfer.[111,112,114,115] While photo-enhanced electrochemical etching generally produces high selectivities for n-GaN over p-GaN but usually creates very rough surface morphologies and is not easy to scale-up to large wafer diameters. In general plasma etching has several advantages over wet chemical etching including anisotropic profiles, critical dimensional control, formation of sub-micron features, cleanliness and repeatability.[95]

High-density plasma etching has proven to be a very effective technique for etching III-Nitrides, particularly as compared to reactive ion etching (RIE). The ability to decouple the ion energy from the ion flux as in an inductively coupled plasma (ICP) reactor has allowed for uniform density and energy distributions to be transferred to the sample while keeping the average ion and electron energy low. This allows for minimum damage while still maintaining fast etch rates. Typical Cl_2/Ar ICP generated plasmas used in etching GaN have etch rates reported to be ~7000 Å/min.[117,118]

Plasma etching occurs through two mechanisms, either by physical sputtering or chemical reaction with the surface or a combination of these two (ion-assisted plasma etching). The physical etch mechanism is predominately by the acceleration of energetic ions formed in the plasma which transfer their energy (generally < 200 eV) and momentum through collisions with the substrate resulting in sputtering of the surface. This process yields the highest degree of anisotropy; however it also produces the greatest amount of etch damage. Rough surface morphology, trenching, poor selectivity, and non-stoichometric surfaces are the consequence of physical sputtering with subsequent reduction in device performance.

In contrast to physical etching, chemical etch mechanisms rely on the creation of reactive species in the plasma that interact with the substrate and form volatile etch products that are then desorbed from the surface. This process is modeled through discreet steps consisting of reactant formation; reactant transport to the substrate surface; adsorption of reactants onto the surface; chemical reaction; and desorption of the volatile etch products from the surface. These processes combine to yield isotropic profiles and low plasma-induced damage because of almost no physical ion bombardment of the

surface. This can however lead to an undercut profile, which may reduce the critical dimensions and reduce its utility for device fabrication. Normally these mechanisms are combined to obtain the 'best of both worlds' through ion-assisted plasma etching, which relies on both physical and chemical mechanisms where the formation of volatile etch products are sputter desorbed. This technique generally results in high etch rates with anisotropic profiles and low surface damage.

2.2.3 Dry Etch Damage

Plasma processes that utilize energetic particles which bombard the semiconductor surface can induce defects in the material that degrade device performance.[98,104-110] These defects that are generated can be much deeper than the range of the energetic ion and can make removing this damage difficult. Ion damage can be measured up to 1000 Å deep even though the ion penetration is less than 10 Å. The damage induced by dry-etching can include defects such as vacancies, interstitials, dislocations or stacking faults, an increase in surface roughness, impurity incorporation (either from ion, mask, or contaminant in the reactor), and device charging effects. These defects can act as traps in the band gap or in the case of GaN; they can contribute electrical activity through the creation of shallow donor states (i.e. nitrogen vacancy). The competition between damage creation and removal of damage by dry etching ultimately determines whether the device has low or high levels of residual damage.[118-120] Slow etch rates have been shown to lead to an accumulation of damage[121] while fast etch rates produce denser but shallower damaged layers closer to the surface.[118]

There are several methods commonly used to characterize etch-induced damage. They fall into one of two general categories: electrical characterization and surface analysis. Electrical measurements are more sensitive to surface damage with capabilities of detecting defect density levels down to 10^9 cm^{-2}.[122-124] Surface analysis can provide information about the physical nature and origins of the defects.[125-127] Electrical analysis techniques such as current-voltage (I-V) and capacitance-voltage (C-V) measurements can be applied to Schottky diodes to obtain parameters related to device performance such as: breakdown voltage (V_{BR}), ideality factor (*n*), barrier height (F_B), and doping profile. This method is commonly employed as Schottky diodes require few processing steps and the rectifying contact is sensitive to plasma damage. Etch-induced damage causes a leakage current through the Schottky diode as illustrated in Figure 10[128]. Here a sheet of etch-induced defects is introduced at the interface between the metal and the semiconductor. Electrons from the semiconductor can tunnel into the unoccupied states in the metal from these defect sites, which creates the additional leakage current in addition to the thermionic emission current.

Etch damage studies have been conducted for both n-and p-type GaN. For n-GaN Schottky diodes it has been found in ICP N and H plasmas that increasing ion energy and increasing ion mass both create greater damage effects such as lowering breakdown voltage (V_{BR}) and increasing leakage current as illustrated in Figure 11.[129] The reduction in the breakdown voltage was found to saturate for ion energies >175 eV.

For p-type GaN Schottky diodes exposed to ICP energetic N or H plasmas there is an increase in breakdown voltage and forward turn-on voltage, with these increases paralleling the increase of source power as seen in Figure 12. The increase in the

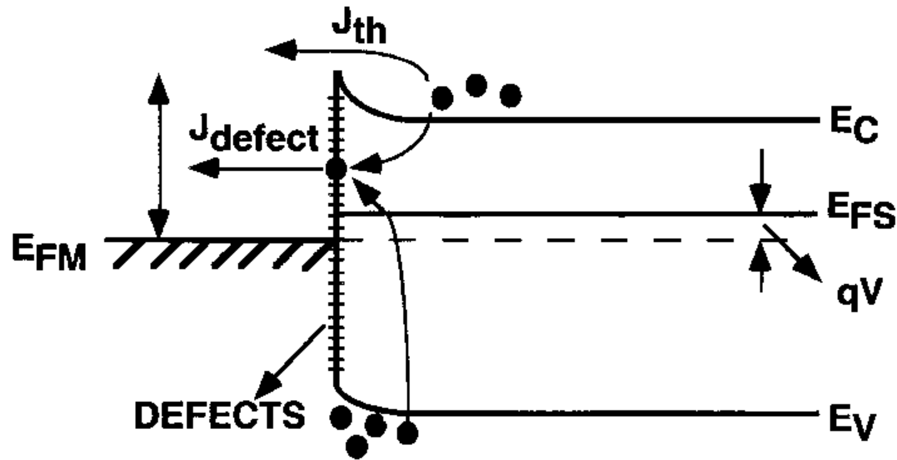

Figure 10 Energy band diagram showing additional leakage current caused by tunneling from defect states in addition to the current created through thermionic emission.

breakdown voltage in the p-GaN is due to a decrease in hole concentration from the near surface area through the creation of shallow donor levels by the plasma damage. In fact, it has been shown that for high source powers ≥ 750 W; the turn-on voltage shows characteristics of an p-n junction, which indicates that the p-type surface is compensated by a shallow defect level with $> 10^{19}$ cm^{-3} donor states as illustrated in Figure 13.[129]

There are several techniques applied to ameliorate the plasma-induced damage in semiconductors. Both wet etching and thermal annealing have been successfully used in GaN for plasma etch-damage removal. However, both of these methods can have drawbacks. Wet etching is less controllable for etch rate or etch profile, and thermal annealing may cause other changes in electrical or mechanical properties due to diffusion of impurities, chemical reactions, and creation of thermal stresses.

When wet etching is used for plasma damage removal, the etch solution should ideally provide a slow etch rate and not cause surface roughening. It is found that

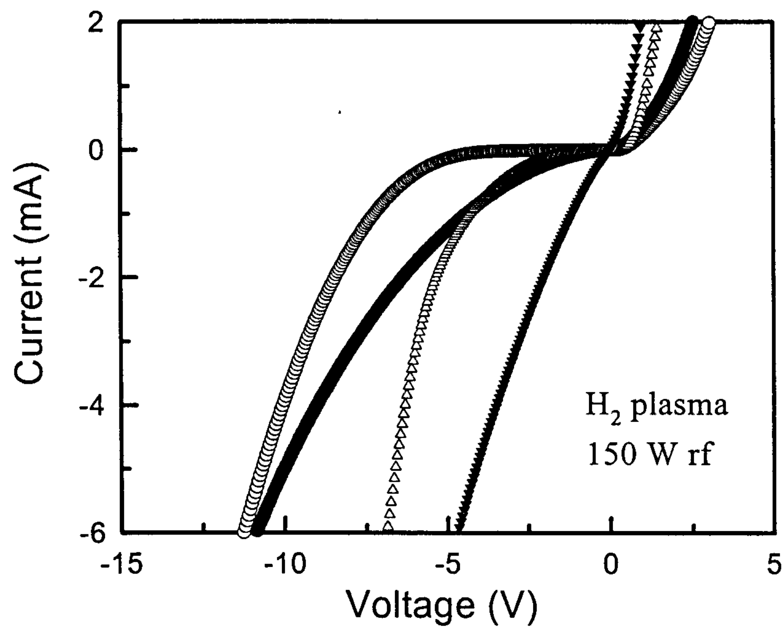

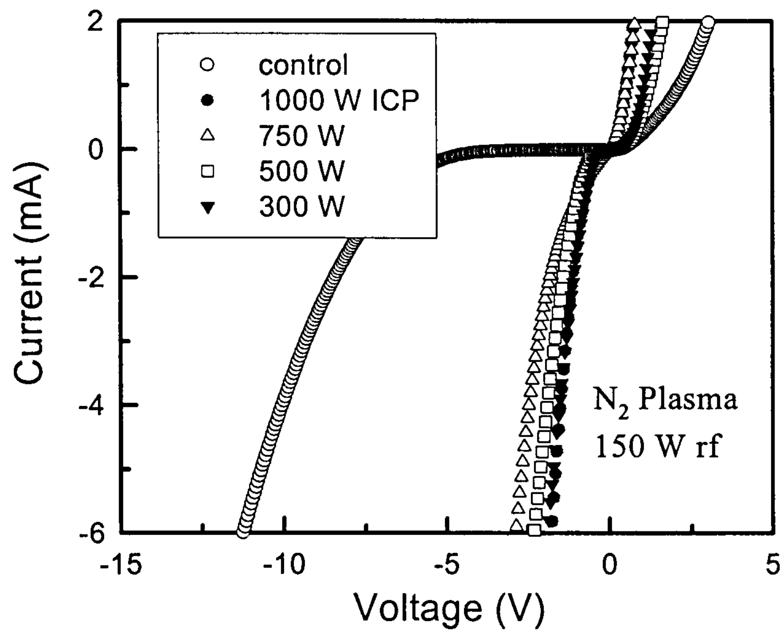

Figure 11 I-V characteristics from n-GaN diodes before and after H_2 (top) and N_2 (bottom) plasma exposure (150 W rf chuck power, 5 mTorr) at different ICP powers.

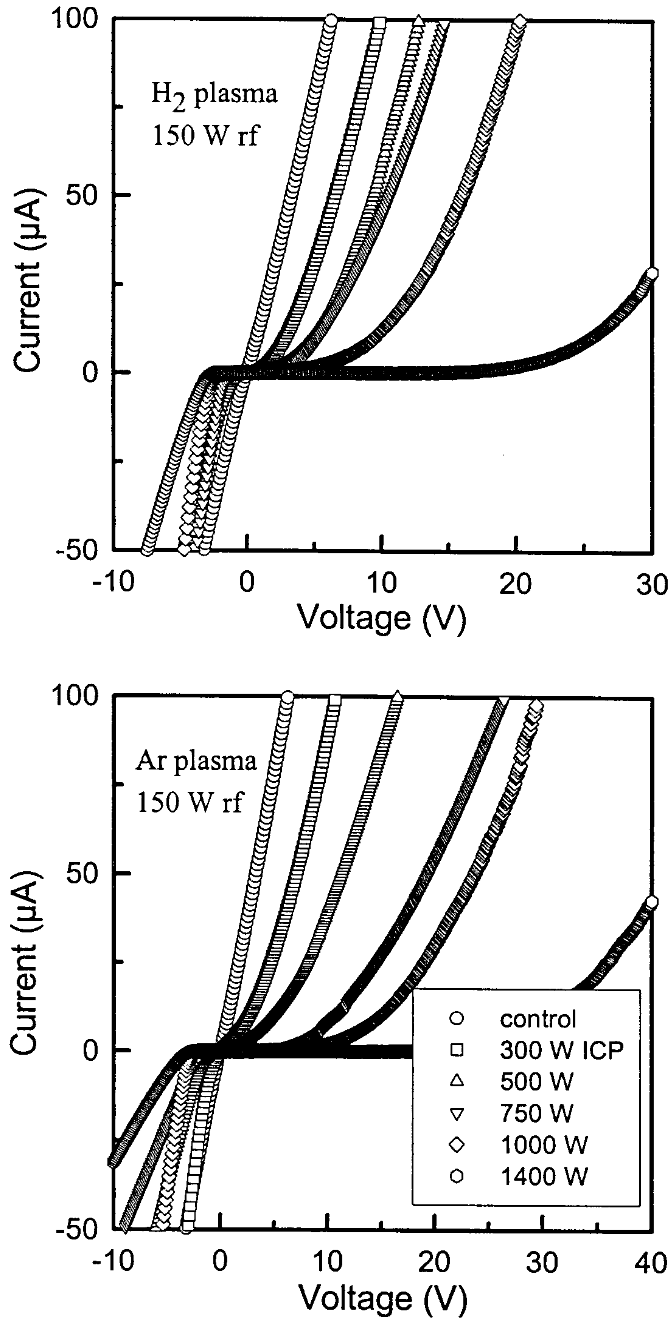

Figure 12 I-V characteristics from p-GaN samples exposed to either H_2 (top) or Ar (bottom) ICP plasma discharges (150 W rf chuck power) as a function of source power prior to deposition of the Schottky contact.

wet etching GaN in a 0.1 M NaOH solution will remove dry-etch damage and restore the breakdown voltage to original levels as illustrated in Figure 14. It is seen that for Ar ICP plasma discharges (500 W source power, 150 W rf chuck power, 1 min, -171 dc chuck bias) that the wet chemical etch treatment will restore the original breakdown voltage of p-GaN within 400-500 Å.[129]

Another effective technique for removing etch-related damage is through thermal annealing. Figure 14 shows the effect of annealing under flowing nitrogen on plasma damaged (750 W source power, 150 rf chuck power, 1 min, Ar discharge) Schottky diodes. The samples were annealed at various temperatures and they show severe compensation at between 500-700°C, however they do return to their original values at 900°C. This is similar to what is experienced in ion-implanted semiconductors where the ion damage creates states that initially compensates the impurity, but at higher annealing conditions this trap density decreases as damage is removed.

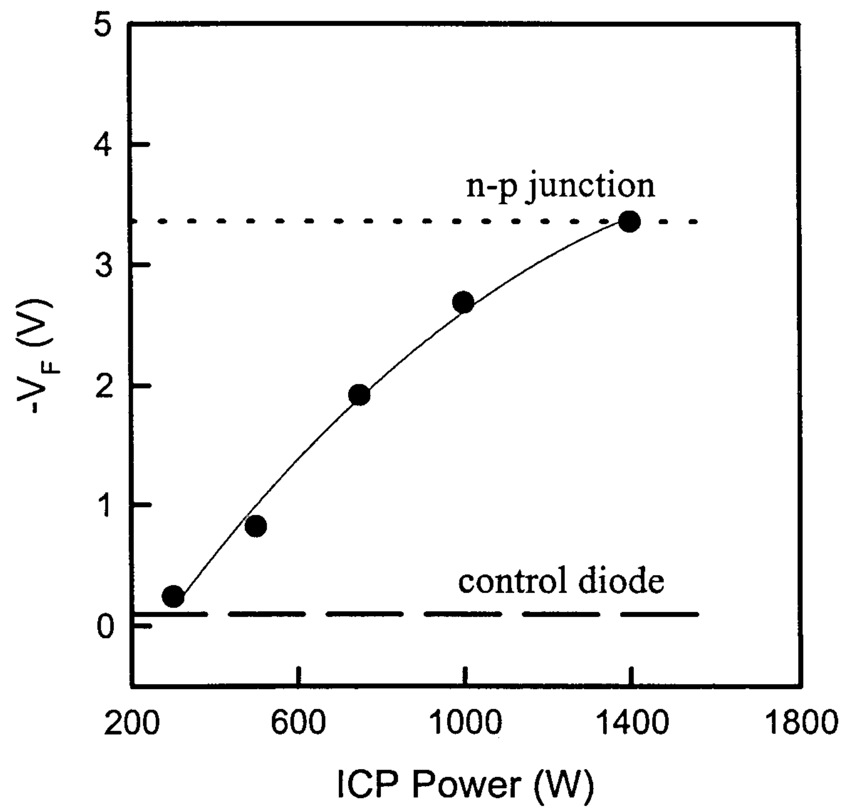

Figure 13 Forward tu ' Ar plasma
discharges (150 W rf)rior to
deposit ion of the Sch

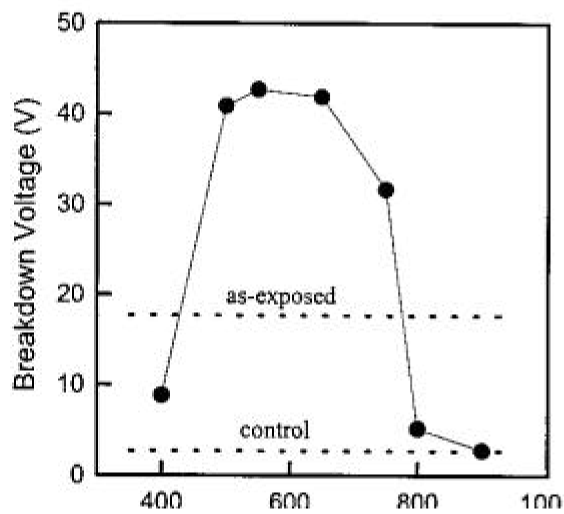

Figure 14 Breakdown voltage as a function of depth removed in a 0.1 M NaOH wet-etch solution for p-GaN diodes (top). Breakdown voltage as a function of thermal annealing temperature for p-GaN diodes (bottom).

58. CHAPTER 3

ELECTRICAL EFFECTS OF N_2 PLASMA EXPOSURE ON DRY ETCH DAMAGE IN P- AND N- GaN SCHOTTKY DIODES

3.1 Materials and Methods

GaN layers 2-3µm thick were grown on c-plane sapphire substrates by Metal Organic Chemical Vapor Deposition at 1050°C. Mg or Si was employed as p- or n-dopants respectively to produce carrier concentrations of 3-5x10^{17} cm^{-3}. To form ohmic contacts, e-beam deposited Ti/Au (for n-type) or Ni/Au (for p-type) was lifted-off and annealed at 750°C for 30 seconds to minimize contact resistance. To produce dry-etch damage in some of these samples, they were exposed to ICP Ar discharges at a source power of 500 W and a rf chuck power of 150 W. These damaged samples were then treated in one of two different ways, namely annealing under flowing N_2 gas or exposure to an N_2 plasma (13.56 MHz, 0.3-1 Torr, 20 min., 20 W) in a Plasma-Therm 790 system. The temperature range explored was 25-350°C. Higher temperatures were found to lead to surface degradation. Schottky contacts were then formed by e-beam deposition of either Pt/Au for n-GaN or Ti/Pt/Au for p-GaN. A schematic of the completed diodes is shown in Figure 15. The current-voltage (I-V) characteristics from the diodes were measured at room temperature.

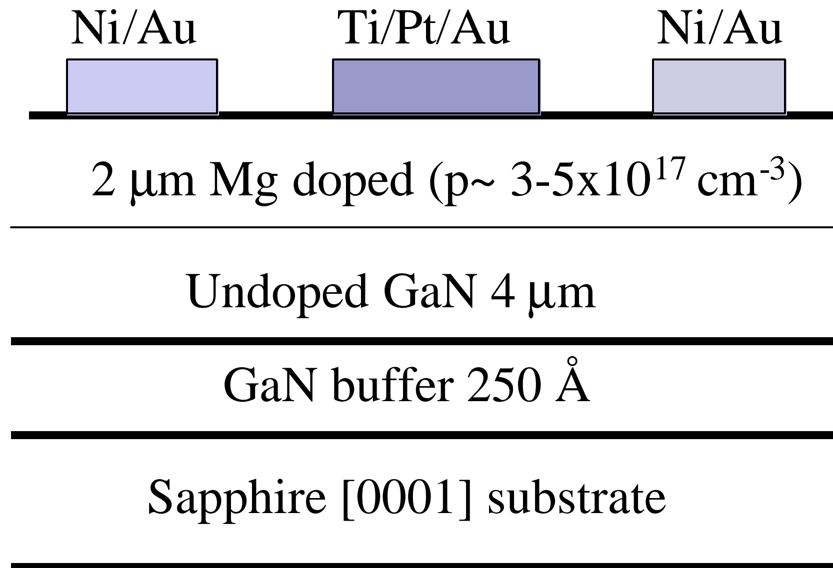
P-type GaN
Ni/Au
Ti/Pt/Au
Ni/Au
2 µm Mg doped (p~ 3-5x10^17 cm^-3)
Undoped GaN 4 µm
GaN buffer 250 Å
Sapphire [0001] substrate

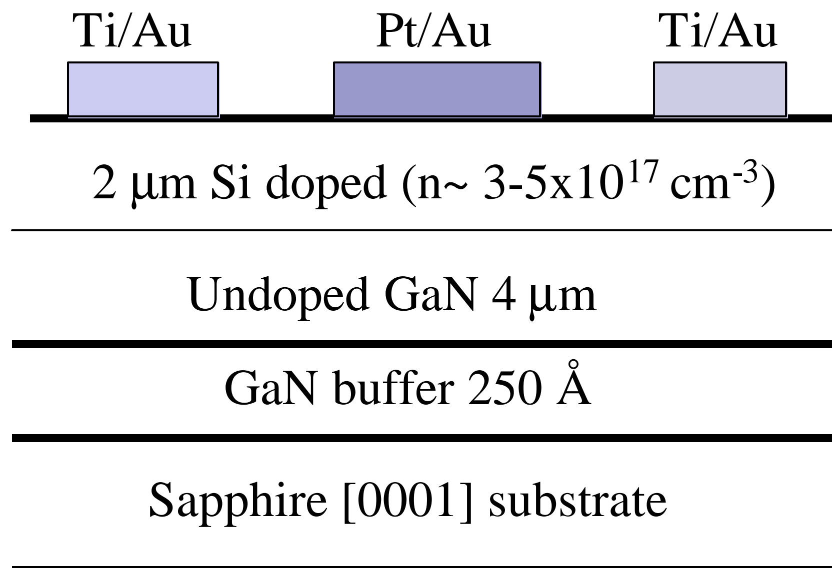
N-type GaN
Ti/Au
Pt/Au
Ti/Au
2 µm Si doped (n~ 3-5x10^17 cm^-3)
Undoped GaN 4 µm
GaN buffer 250 Å
Sapphire [0001] substrate

3.2 Results and Discussion

Figure 16 shows I-V characteristics from n-GaN diodes before and after the initial Ar plasma damage and subsequent N_2 plasma exposure. Figure 17 shows a comparison of N_2 plasma exposure and simple annealing at different temperatures. There are some important features of the data. First, it is clear that the Ar plasma damage greatly degrades the reverse breakdown voltage (V_B). Second, there is some recovery of V_B for both N_2 plasma treatments and annealing, with larger recoveries at higher temperatures. Third, a comparison of the two sets of data shows that there is a greater improvement in V_B with N_2 plasma exposure relative to annealing at the same temperature. This suggests the presence of a chemical mechanism in the damage recovery, which is plausible given that creation of nitrogen vacancies is thought to be a major component of etch damage in GaN.[96,104,106,107] Fourth, there is not complete recovery of the V_B values at any of the temperatures we investigated. When we tried higher temperature N_2 plasma exposures, the GaN surfaces were badly degraded.

Figure 18 shows the effect of N_2 plasma process pressure on the I-V characteristics of n-GaN diodes for 350°C exposures. Within experimental error there is no difference in the V_B values. Since the neutral atomic nitrogen density is larger at higher pressures, it is clear that this neutral flux incident on the GaN surface is not limiting the damage recovery process. The relative contributions of annealing and nitridation to the recovery in V_B can be seen in Figure 19 for the n-GaN diodes. There was also observed a smoothing of the n-GaN surface upon N_2 plasma exposure, as shown

Figure 15 Schematic of p-type planar Schottky diode structure (top), or n-type planar Schottky diode structure (bottom).

in the Atomic Force Microscopy (AFM) scans of Figure 20. A similar effect was also reported by Lee et. al.[113]

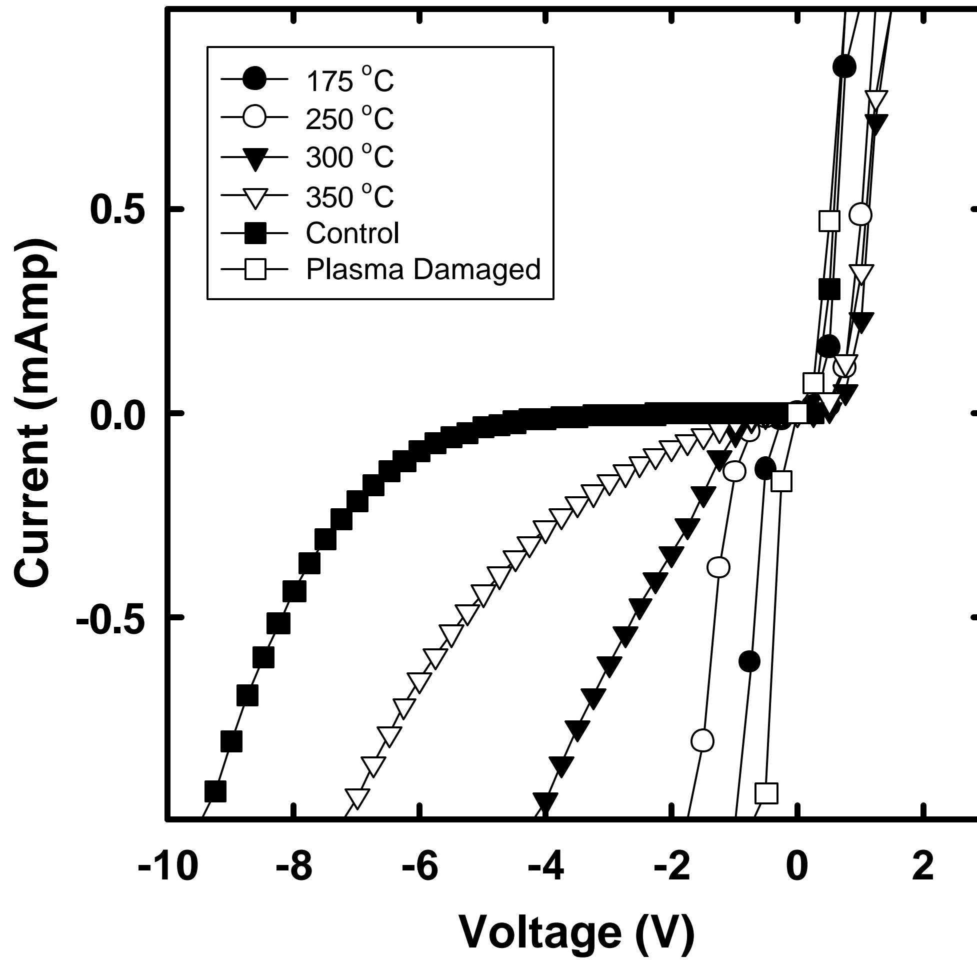

Figure 16 I-V characteristics from n-GaN diodes before and after Ar plasma damage and subsequent N_2 plasma exposure at different temperatures.

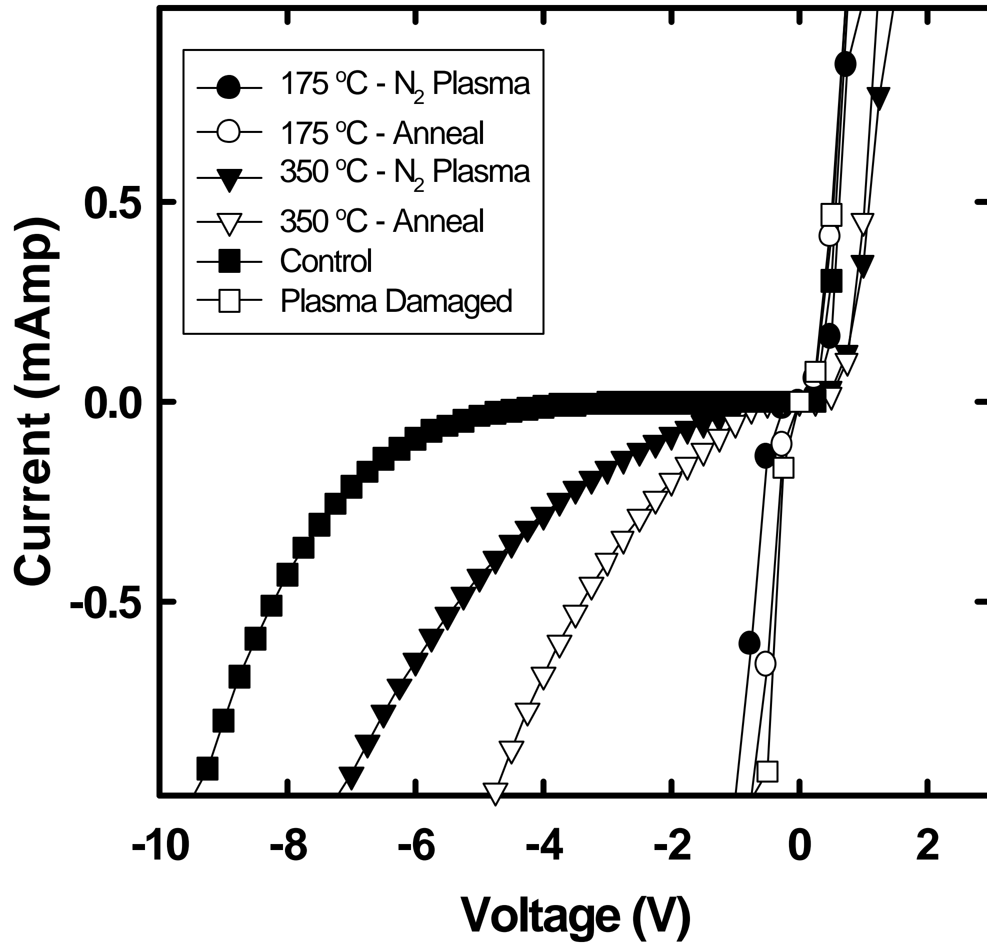

Figure 17 I-V characteristics from n-GaN diodes comparing N_2 plasma exposure and annealing at the same temperatures.

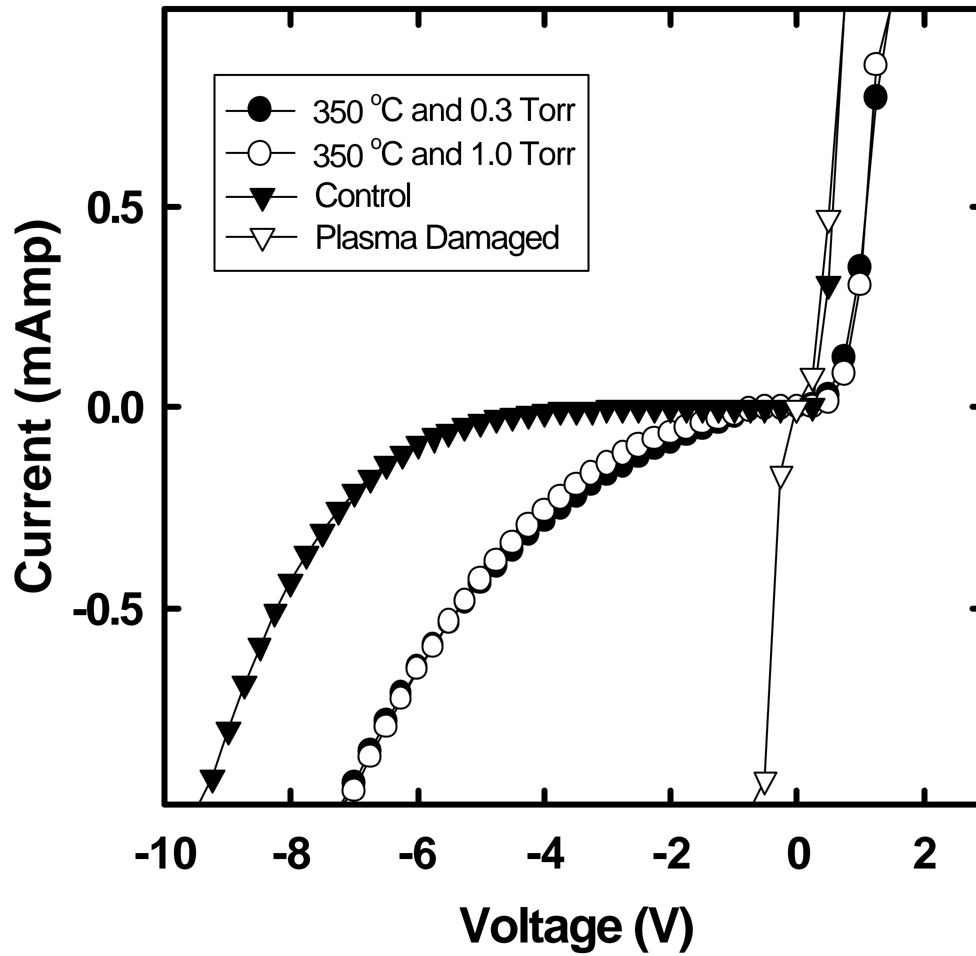

Figure 18 I-V characteristics from n-GaN diodes before and after Ar plasma damage and subsequent N_2 plasma exposure at 350°C and different pressures.

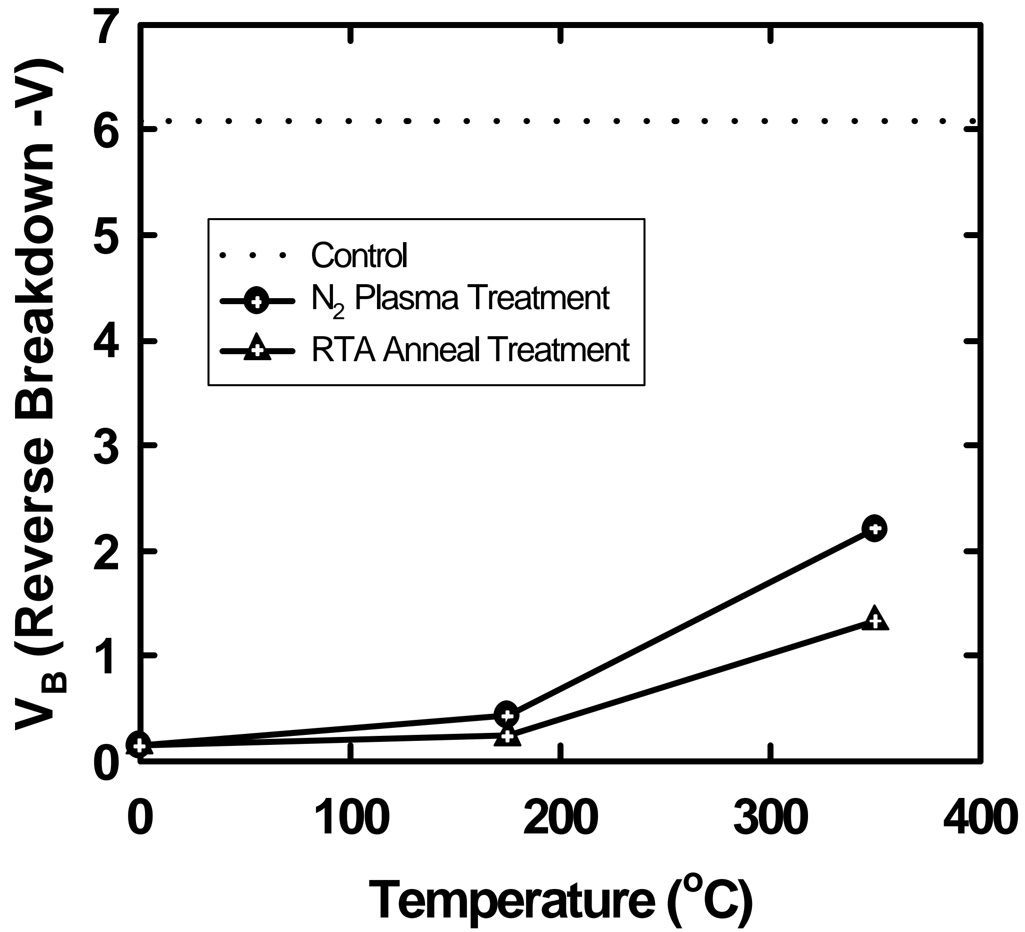

Figure 19 N-GaN diodes showing plot of V_B versus treatment temperature for N_2 plasma exposure or annealing.

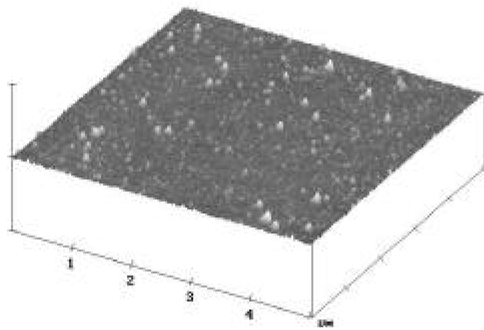

Control
RMS Roughness: 1.18

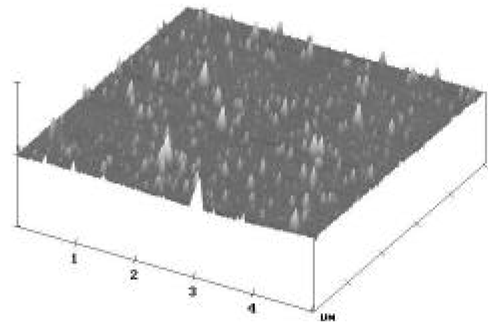

Plasma Damaged
RMS Roughness: 2.35

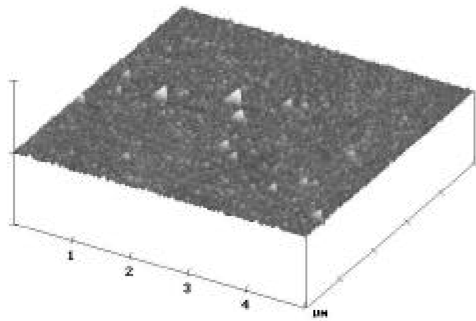

N_2 Plasma Treatment at 175 ^oC
RMS Roughness: 1.47

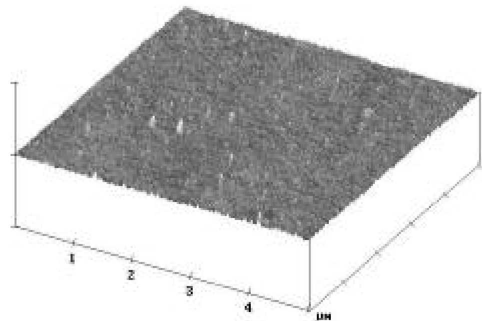

N_2 Plasma Treatment at 350 ^oC
RMS Roughness: 1.35

Figure 20 AFM scans of n-GaN surface before and after Ar plasma damage and after subsequent N_2 plasma treatment.

Turning to the p-type GaN, Figure 21 shows I-V characteristics from diodes before and when the initial Ar plasma exposure and subsequent N_2 plasma exposure at various process temperature. Figure 22 shows a comparison of these results with conventional annealing at the same temperatures. The initial plasma damage causes an increase in V_B, which has been ascribed to a decrease in the p-type conductivity.[107] The influence of the substrate temperature is much different for p-GaN than for the n-type material. The largest recovery in the I-V characteristics was observed for 175°C N_2 plasma exposures or anneals and in fact annealing at 350°C increased V_B. This is consistent with previous results showing that V_B of p-GaN diodes initially decreases with annealing, then increases at higher temperatures before decreasing back near the original value at ~ 900°C.[107] The differences between n- and p-type material suggest a strong Fermi-level dependence to annealing of plasma-induced defects in GaN. The key result in Figure 21 is that N_2 plasma exposure is not an effective method for damage removal in p-GaN.

Figure 23 shows that process pressure during N_2 plasma exposure at 350°C has a significant effect on the I-V characteristics of p-GaN diodes. However, none of the conditions produced acceptable recovery of breakdown voltage. A summary of the V_B values before and after Ar plasma damage and after annealing or nitridation at different temperatures is shown in Figure 24.

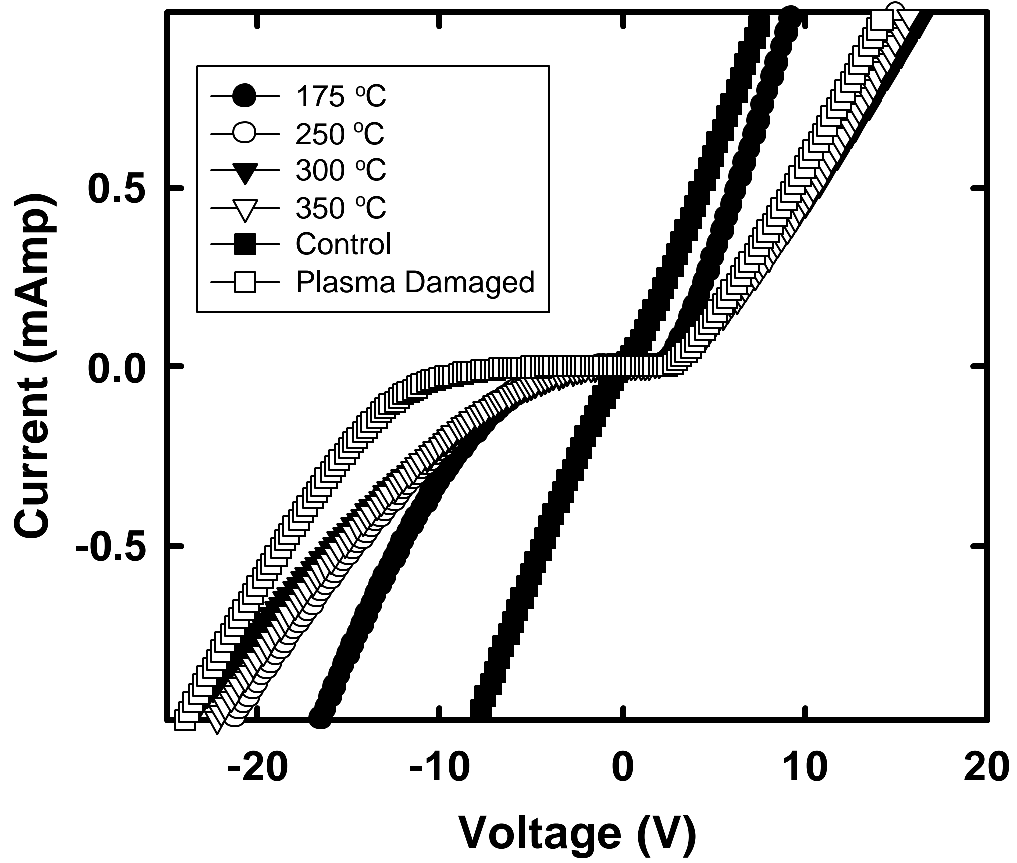

Figure 21 I-V characteristics from p-GaN diodes before and after Ar plasma damage and subsequent N_2 plasma exposure at different temperatures.

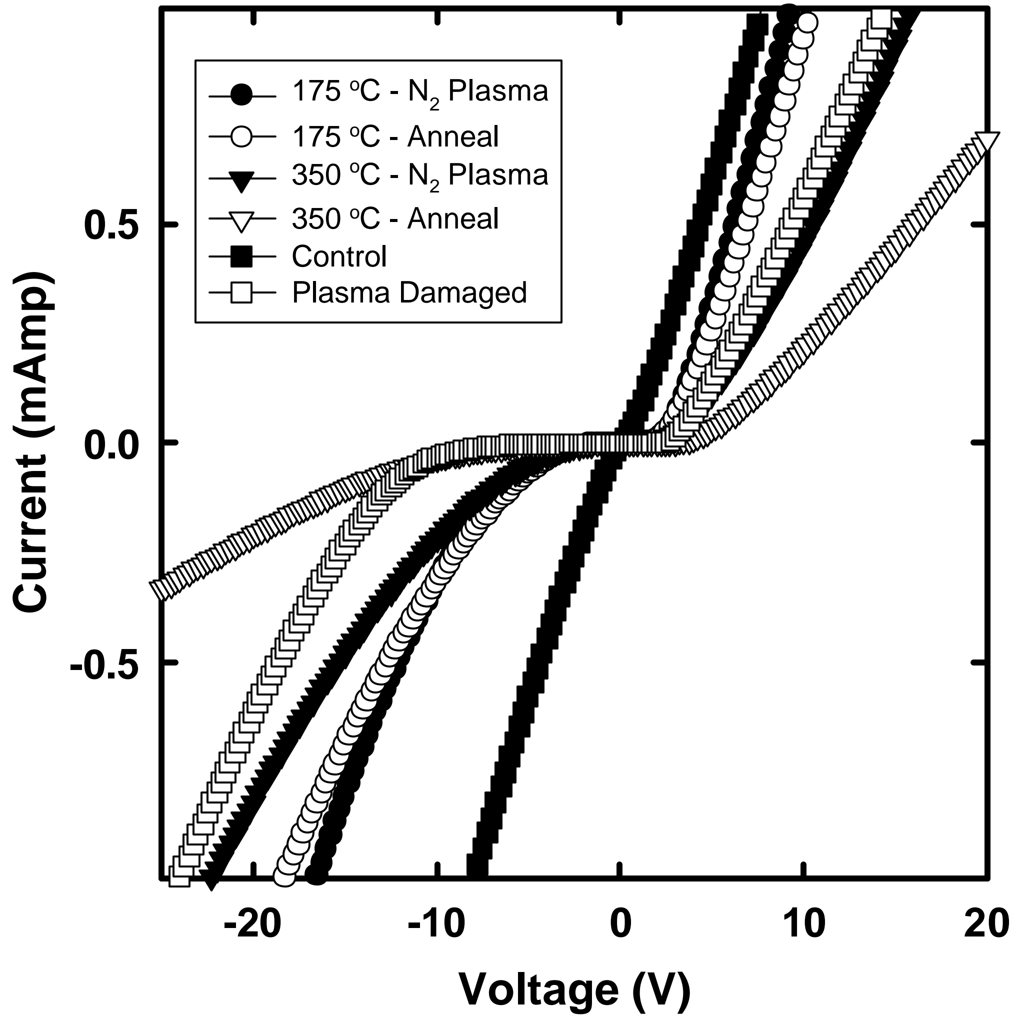

Figure 22 I-V characteristics from p-GaN diodes comparing N_2 plasma exposure and annealing at the same temperatures.

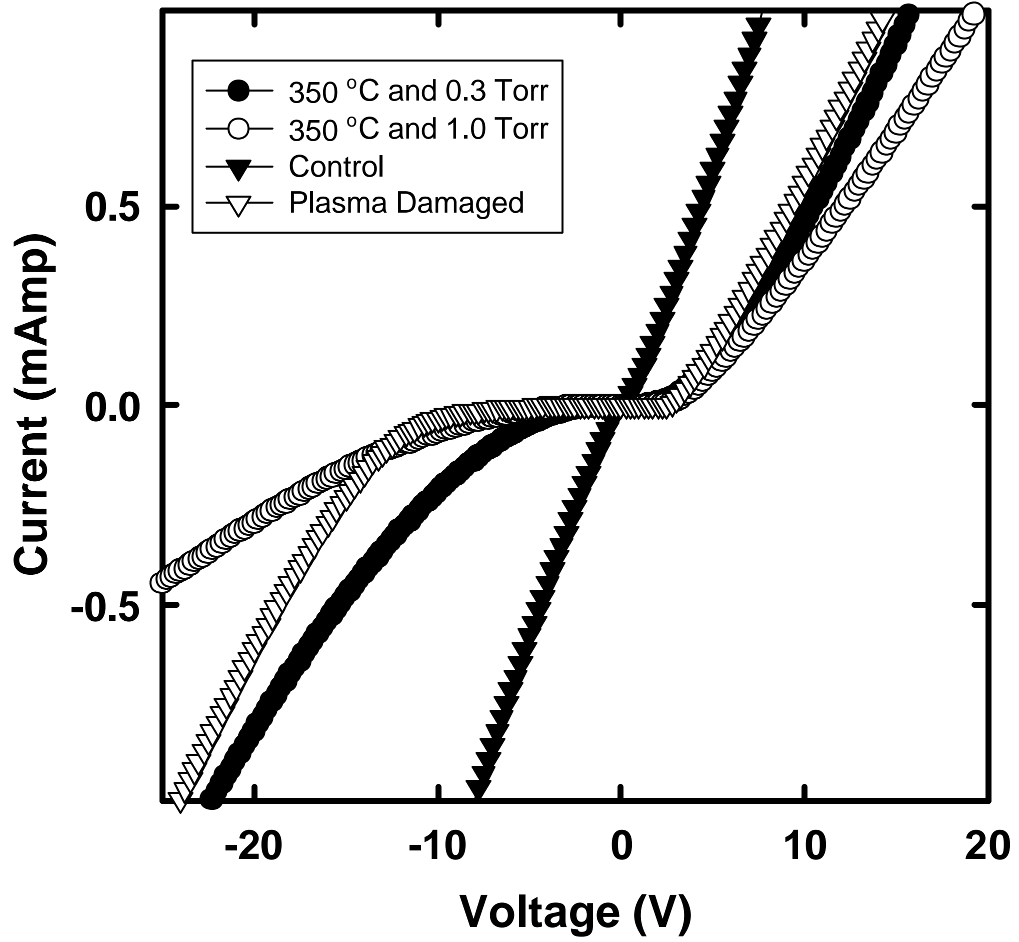

Figure 23 I-V characteristics from p-GaN diodes before and after Ar plasma damage and subsequent N_2 plasma exposure at 350°C and different pressures.

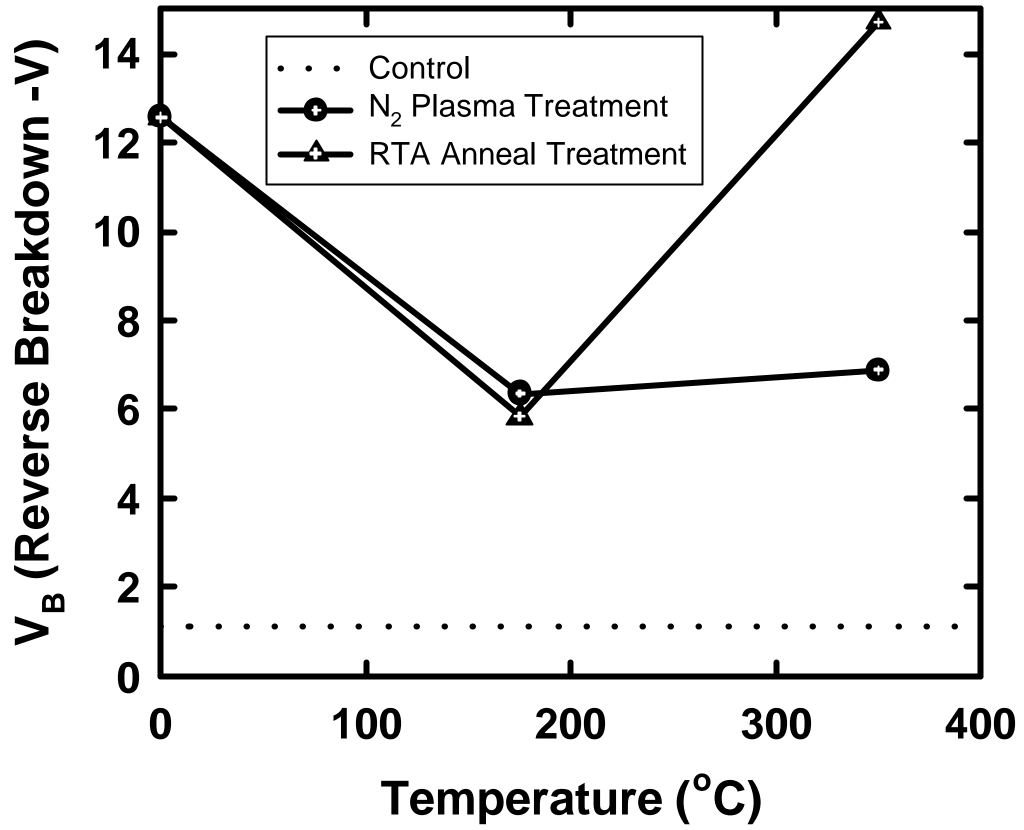

Figure 24 P-GaN diodes showing plot of V_B versus treatment temperature for N_2 plasma exposure or annealing.

4.1 Materials and Methods

Undoped GaN samples were grown on c-plane Al_2O_3 substrates by rf-plasma activated Molecular Beam Epitaxy to a total thickness of 2µm. The samples displayed a low ($3x10^{15}$ cm^{-3}) n-type background carrier concentration. Multiple energy Be^+ or Mg^+ implants were performed in a non-channeling direction to total doses of $1.65x10^{15}$ cm^{-2} and $1.70x10^{15}$ cm^{-2} respectively to produce average volume concentrations of $5.03x10^{19}$ cm^{-3} to a depth of 0.3 µm. Oxygen implants were performed in a similar manner to produce uniform volume concentrations corresponding to half, equal or double the Be or Mg concentrations. Simulated ion profiles of GaN with Be + O or Mg + O implants are shown in Figure 25 and 26 respectively. This precise control of the ratio of donors (oxygen) to acceptors (beryllium and magnesium) is an important advantage of the implant process. Sections from the samples were then annealed at 950-1150°C for 10

CHAPTER 4
CO-IMPLANTATION OF Be + O AND Mg + O INTO GaN

seconds under a flowing N_2 ambient with the implanted face covered by another GaN wafer. Hall measurements at room temperature were performed by alloying HgIn eutectic contacts (420°C, 300 seconds) to the corners of 3x3 mm^2 sections.

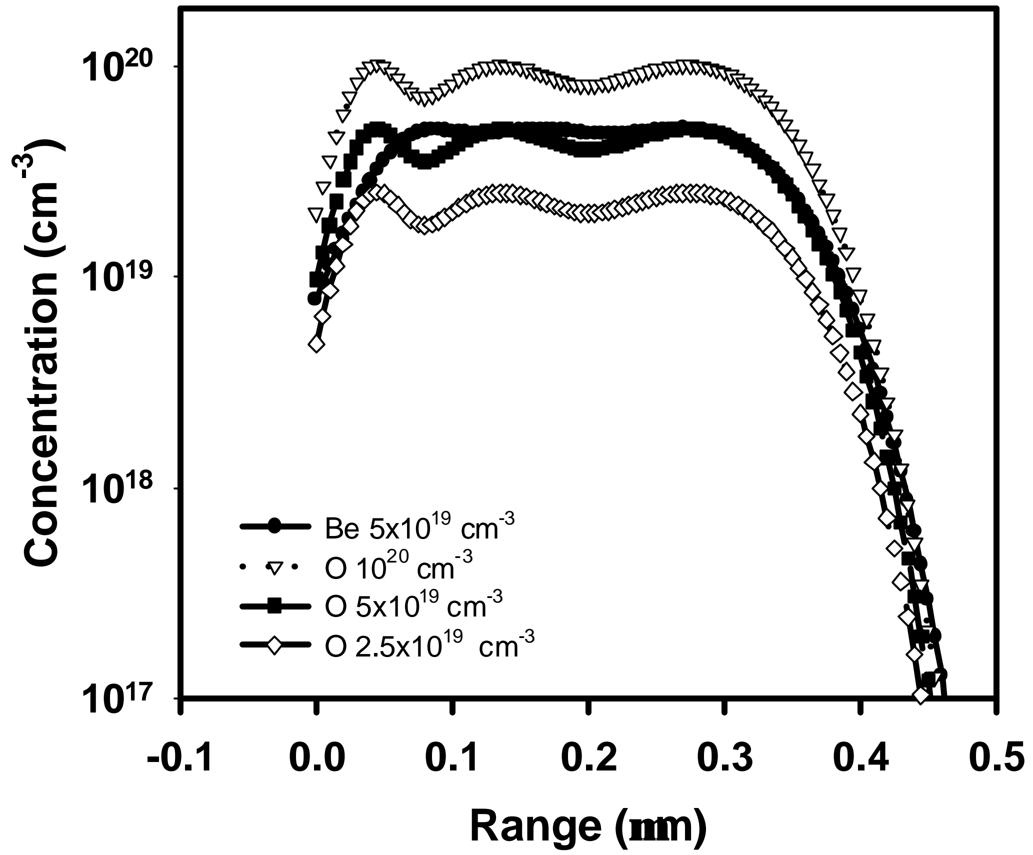

Figure 25 Simulated Be implant ion profile in GaN with multiple-energy O co-implants.

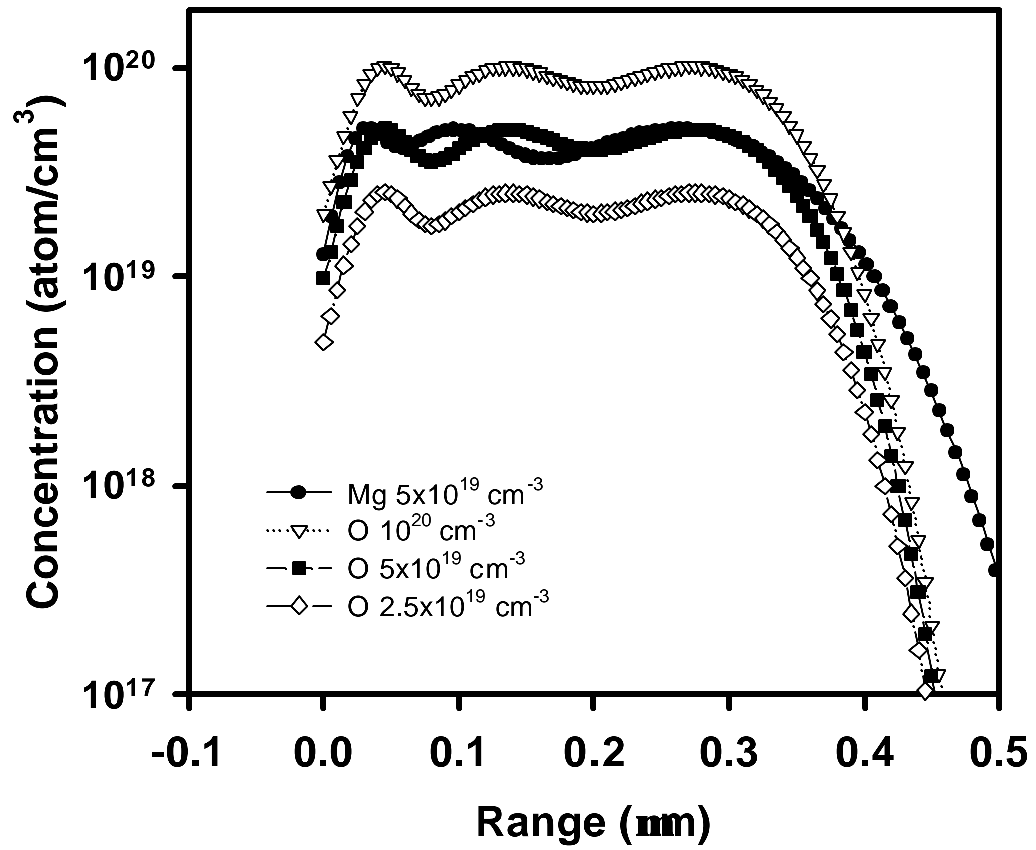

Figure 26 Simulated Mg implant ion profile in GaN with multiple-energy O co-implants.

4.2 Results and Discussion

(a) Be + O implants

A summary of the electrical data for the annealed Be + O implanted samples is shown in Table 3(a). The variation of sheet resistance versus temperature is shown in Figure 27, while mobility versus temperature are shown in Figure 28. There are several important features of the data. Firstly for an O|Be ratio of 0.5, the activated samples are high-resistivity, p-type only for anneal temperatures ≤1000°C. At higher temperatures there is type conversion to n-type, which might be due to Be atoms coming out of solution or to more efficient activation of the O donors. At an O|Be ratio of 1 the best p-type concentration is obtained for 950°C annealing. However the sheet carrier concentration under these conditions (3.8×10^{12} cm^{-2}) is about a factor of 3 lower than reported in ref. 93 for Be-only implants into GaN. The sheet carrier density decreases with higher annealing temperatures and converts to n-type for 1100°C anneals. At an O|Be ratio of 2, very high sheet hole densities are achieved for anneals at 1050-1100°C, with an active hole fraction of ~10%. This is higher than expected from the reported ionization energy of 0.127 eV, which would lead to an active hole fraction of ~1% at room temperature. This data is more consistent with the predictions of refs 88,89 and 94 of a shallow ionization level for Be paired with O in GaN.

We attempted to measure the activation energy for Be to become electronically active when implanted in GaN. The data for sheet carrier concentration versus anneal temperature for three different O|Be ratios is shown in Figure 29, while the

Arrhenius plot is shown in Figure 30. There are no linear portions for any of the plots in the latter

	Anneal Temp(°C)	O Conc. (cm^{-3})	Type	Restivity (W-cm)	Mobility (cm^{2}V^{-1}s^{-1})	Conc. (cm^{-3})	Sheet Res. r (W/q)	Sheet Conc. (cm^{-2})
(a) Be, Total Dose = ~1.65x10^{15}cm^{-2} Averge Concentration = ~5x10^{19} cm^{-3}	950	5.1E+19	P	19.6	2.5	1.3E+17	6.5E+05	3.8E+12
	1000	5.1E+19	P	27.9	3.2	7.6E+16	9.3E+05	2.3E+12
	1050	5.1E+19	P	35.3	11.5	1.6E+16	1.2E+06	4.8E+11
	1100	5.1E+19	N	11.4	578.4	2.0E+15	3.8E+05	6.1E+10
	1150	5.1E+19	N	54.2	10.3	1.1E+16	1.8E+06	3.4E+11
	950	2.5E+19	P	269.7	68.8	4.2E+14	9.0E+06	1.3E+10
	1000	2.5E+19	P	226.5	75.0	3.9E+14	7.6E+06	1.2E+10
	1050	2.5E+19	N	194.9	15.3	7.4E+15	6.5E+06	2.2E+11
	1100	2.5E+19	N	8.4	285.5	8.1E+15	2.8E+05	2.4E+11
	1150	2.5E+19	N	3.8	153.6	2.4E+16	1.3E+05	7.3E+11
	950	1.0E+20	P	75.9	8.2	1.1E+16	2.5E+06	3.2E+11
	1000	1.0E+20	P	42.6	3.9	1.4E+17	1.4E+06	4.3E+12
	1050	1.0E+20	P	11.2	1.8	6.9E+18	3.7E+05	2.1E+14
	1100	1.0E+20	P	4.1	1.5	3.4E+18	1.4E+05	1.0E+14
	1150	1.0E+20	N	8.4	60.2	1.8E+16	2.8E+05	5.3E+11
(b) Mg, Total Dose = ~1.70x10^{15} cm^{-2} Average Concentration = ~5x10^{19} cm^{-3}	950	5.1E+19	N	21.7	6.3	6.9E+16	7.2E+05	2.1E+12
	1000	5.1E+19	N	38.8	15.7	1.2E+16	1.3E+06	3.5E+11
	1050	5.1E+19	N	10.4	9.2	6.5E+16	3.5E+05	2.0E+12
	1100	5.1E+19	N	12.3	28.5	2.2E+16	4.1E+05	6.5E+11
	1150	5.1E+19	N	8.2	4.7	1.6E+17	2.7E+05	4.8E+12
	950	2.5E+19	N	37.3	11.3	1.5E+16	1.2E+06	4.6E+11
	1000	2.5E+19	N	27.9	31.5	7.1E+15	9.3E+05	2.1E+11
	1050	2.5E+19	N	26.0	3.8	2.4E+17	8.7E+05	7.1E+12
	1100	2.5E+19	N	14.2	87.9	7.8E+15	4.7E+05	2.3E+11
	1150	2.5E+19	N	77.2	796.2	4.2E+14	2.6E+06	1.2E+10
	950	1.0E+20	N	45.3	23.2	6.1E+15	1.5E+06	1.8E+11
	1000	1.0E+20	N	45.2	58.9	3.2E+15	1.5E+06	9.7E+10
	1050	1.0E+20	N	23.8	11.6	3.7E+17	7.9E+05	1.1E+13
	1100	1.0E+20	N	25.0	27.7	9.0E+15	8.3E+05	2.7E+11
	1150	1.0E+20	N	161.7	37.5	1.1E+15	5.4E+06	3.3E+10

Table 3 Summary of electrical data for Be + O (a) and Mg + O (b) implanted samples in GaN.

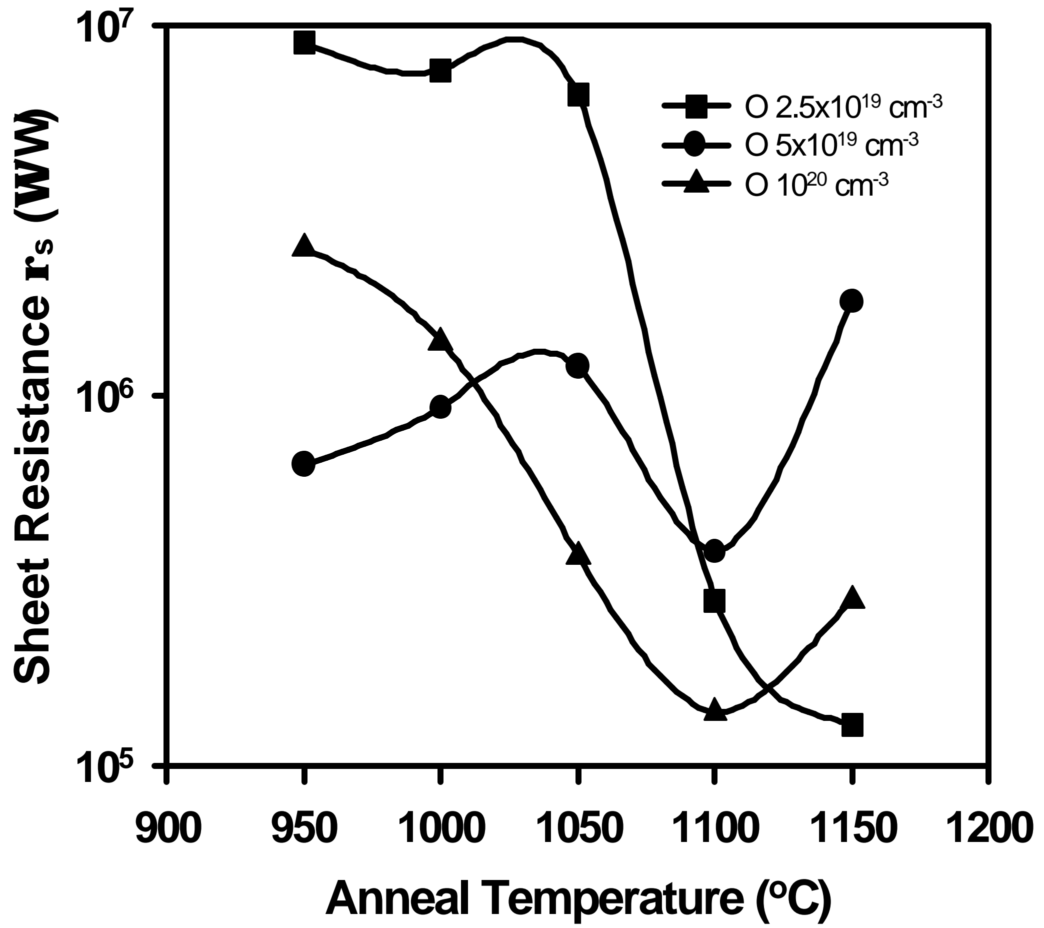

Figure 27 Sheet resistance as a function of anneal temperature in Be + O co-implanted GaN.

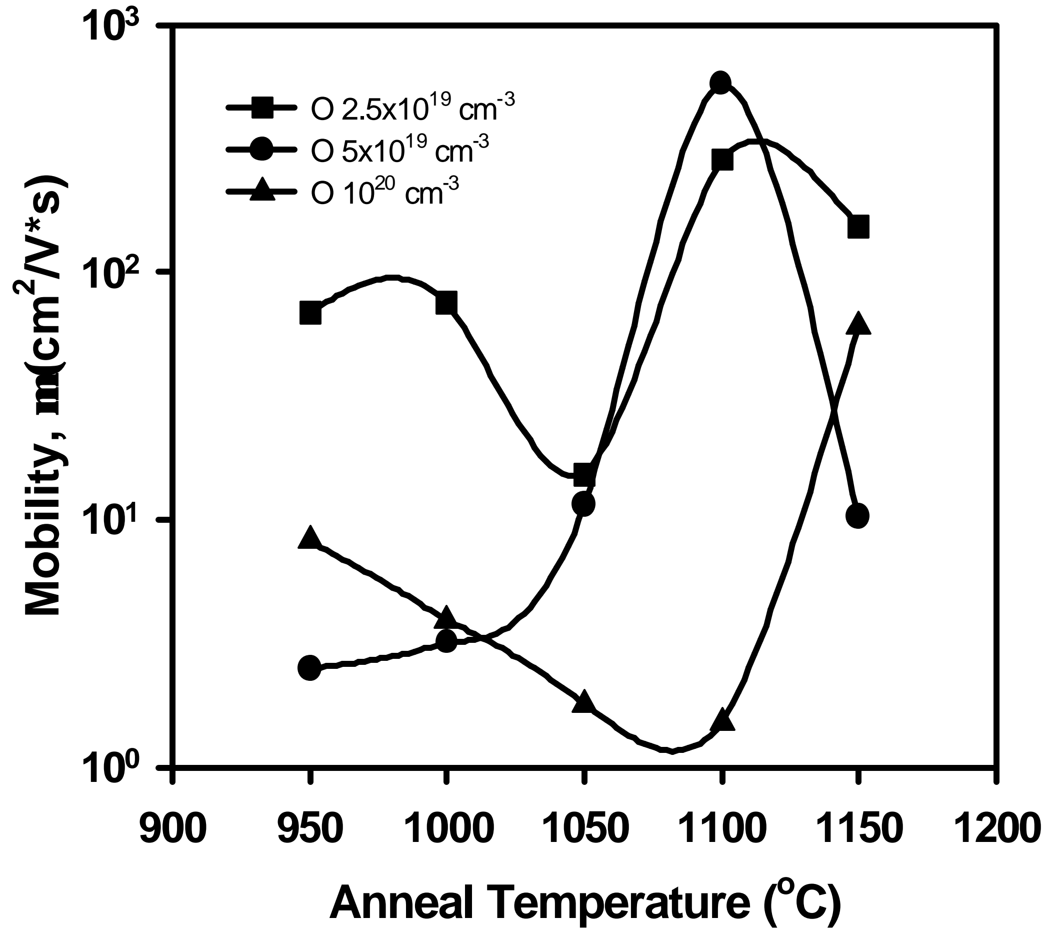

Figure 28 Mobility as a function of anneal temperature in Be + O co-implanted GaN.

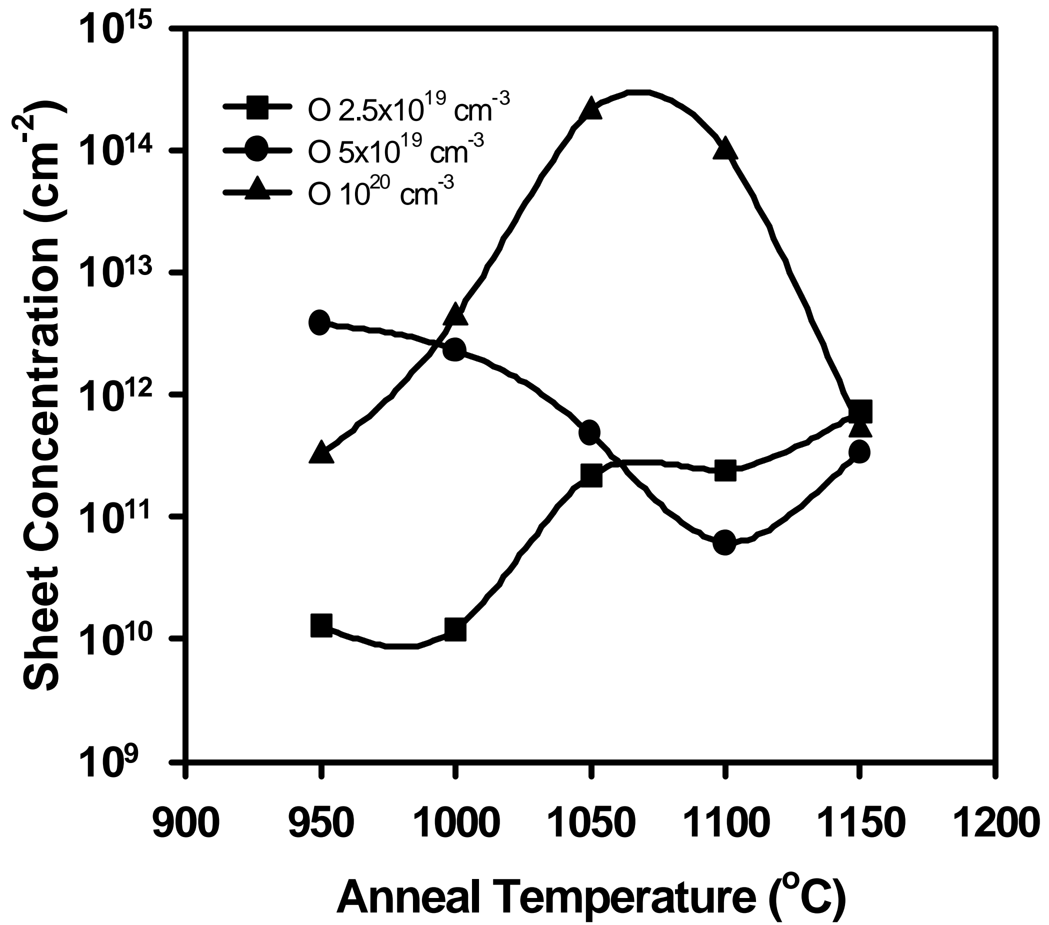

Figure 29 Sheet carrier concentration as a function of anneal temperature in Be + O co-implanted GaN.

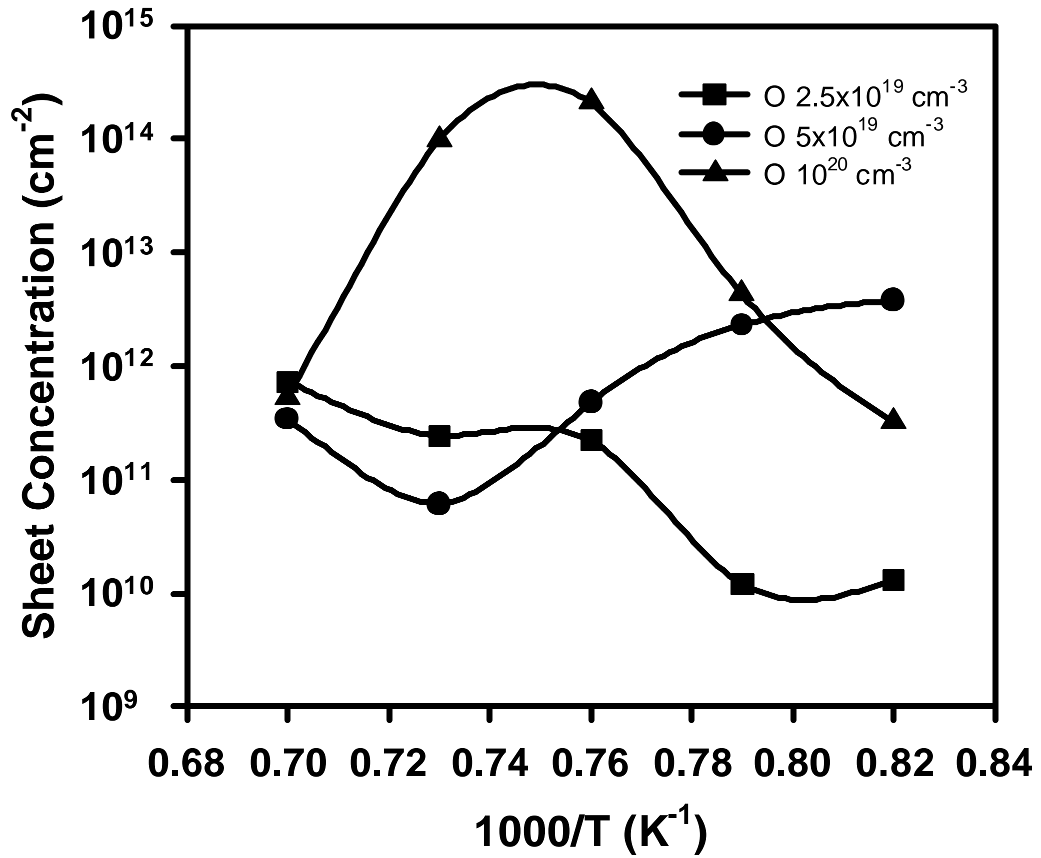

Figure 30 Sheet carrier concentration as a function of anneal temperature in Be + O co-implanted GaN in Arrhenius form.

case, suggesting that the activation is not a simple, single-step process involving movement of Be interstitials into the Ga sub-lattice. The complex behavior evident from Figure 30 indicates there are multiple processes occurring, involving activation of the O, annealing of damage-related donors and possibly pairing of Be and O.

(b) Mg + O co-implants

A summary of the electrical characteristics of the Mg + O implanted samples after annealing is shown in Table 3(b). In all cases, the samples remained n-type with relatively high resistivity. This is consistent with previous photoconductivity experiments in which bulk GaN doped with Mg and O was highly compensated.[130] In that case it was suggested that if Mg and O combined to form molecular doping with a bonding energy larger than that of Ga to N in GaN, the energy levels due to Mg-O complexes would be outside the GaN bandgap. Figure 31 shows the variation of sheet carrier density and Figure 32 shows the variation in carrier mobility with annealing temperature in the Mg + O implanted GaN. In all cases the sheet density remained low ($\leq 10^{13}$ cm^{-2}) relative to the Mg implant dose (1.7×10^{15} cm^{-2}).

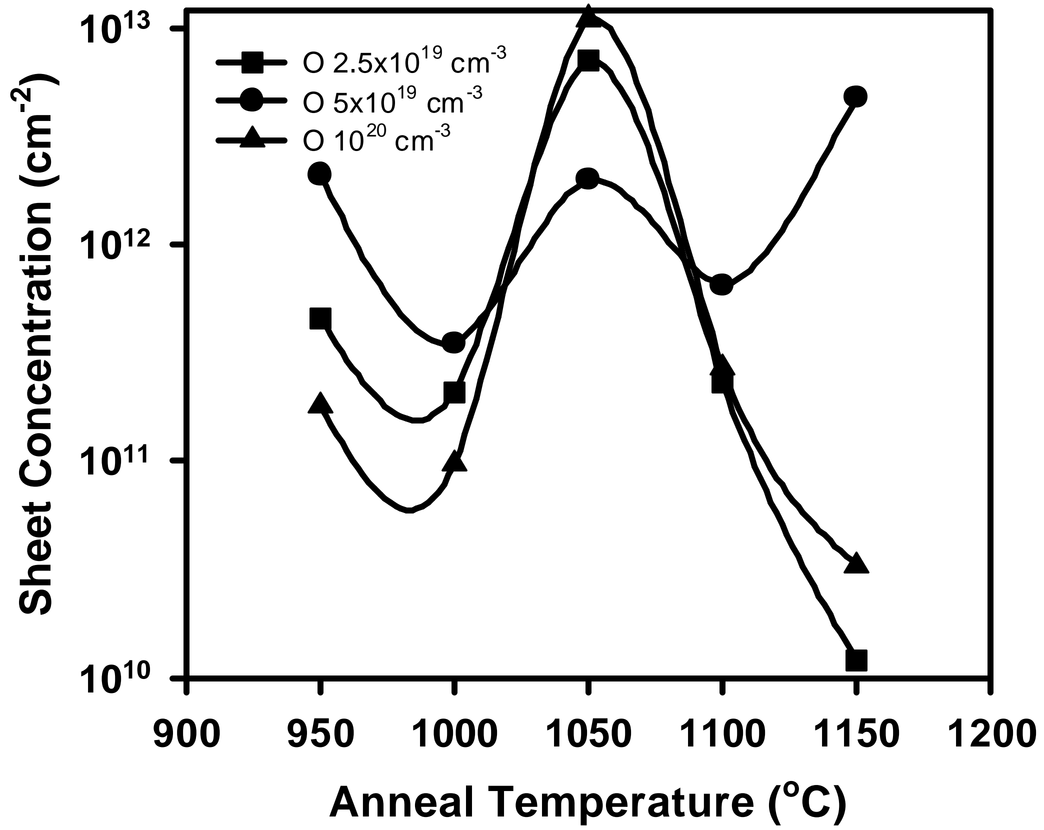

Figure 31 Sheet carrier concentration as a function of anneal temperature in Mg + O co-implanted GaN.

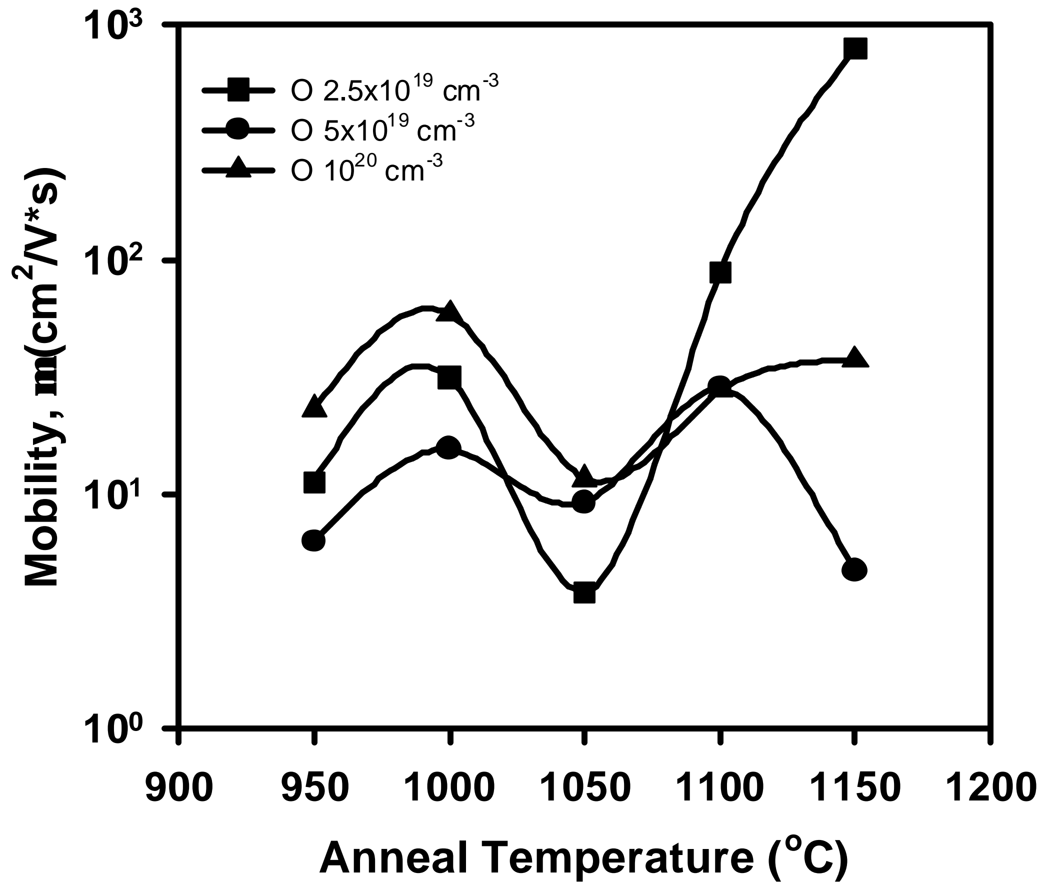

Figure 32 Mobility as a function of anneal temperature in Mg + O co-implanted GaN.

CHAPTER 5
SUMMARY

From the very early days of doping semiconductors it has been realized that co-doping with donors and acceptors increases the solubility of both types of impurity beyond the solubility limit of either impurity in the host semiconductor.[90] Brandt et al.[91] achieved good activation of Be in Be + O co doped GaN grown by MBE with unusually high mobilities resulting form the lower scattering cross-section for holes of the Be-O centers relative to Be acceptors. We observe good activation of Be in Be + O co-implanted GaN for a donor/acceptor ratio of 2. This is a higher ratio than predicted in refs 88 and 89, but this may be related to the low activation efficiency of implanted O in GaN.[9,79] Our data is consistent with an ionization energy for Be of $\leq$ 100 meV, in line with recent photoluminescence results.[132,133] By contrast, under our conditions, Mg + O co-implantation was ineffective in improving the hole density.

Removal of dry etch damage in GaN, especially p-type material, is critical to the performance of a number of electronic devices, including bipolar transistors and mesa rectifiers. Since at least part of the dry etch damage consists of a nitrogen deficiency in

the near-surface region, it is plausible that nitridation of this surface by exposure to a N_2 plasma might aid in damage recovery. However our results show that in the temperature range up to 350°C, N_2 plasma exposure produces only partial recovery of reverse breakdown voltage in Schottky diode structures on both conductivity types of GaN. The recovery originates in at least two mechanisms; a simple annealing of point defect damage and a chemical effect from reactive nitrogen in the plasma. It still appears that either high temperature annealing or wet etch removal of the damaged region is necessary to achieve full recovery of the electrical properties of the GaN surface.

REFERENCES

1. H. Amano, M. Kito, K. Hiramatsu and I. Akasaki, Jpn. J. Appl. Phys. 28 L2112 (1989).

2. R. V. Steele, "Update on GaN Technology and Markets." Compound Semiconductor. July 2000: 14-15.

3. F. A. Ponce and D. P. Bour, Nature 386 351 (1997).

4. F. Ren, C. R. Abernathy, J. D. Mackenzie, B. P. Gila, S. J. Pearton, M. Hong, M. A. Marcus, M. J. Schurman, A. G. Baca and R. J. Shul, Solid-State Elec. 42 2177 (1998).

5. M. S. Shur, Solid-State Elec. 42 2131 (1998).

6. E. R. Brown, Solid-State Elec. 42 2119 (1998).

7. Z. Z. Bandic, E. C. Piquette, P. M. Bridger, R. R. Beach, T. F. Keuch and T. C. Mcgill, Solid-State Elec. 42 2289 (1998).

8. J. C. Zolper, Solid-State Elec. 42 2153 (1998).

9. S. J. Pearton, J. C. Zolper, R. J. Shul and F. Ren, J. Appl. Phys. 86 1 (1999).

10. S. D. Lester, F. A. Ponce, M. G. Craford and D. A. Steigerwald, Appl. Phys. Lett. 66 1249 (1995).

11. S. Nakamura and G. Fasol, The Blue Laser Diode. Berlin: Springer, (1997).

12. I. Grzegory and S. Porowski, in: Properties, Processing and Applications of Gallium Nitride and Related Semiconductors. eds. J. Edgar, S. Strite, I. Akasaki, H. Amano and C. Wetzel. London: IEE INSPEC (1999).

13. H. Amano, N. Sawaki, I. Akasaki and Y. Toyoda, Appl. Phys. Lett. 48 353 (1986).

65

14. Y. Kato, S. Kitamura, K. Hiramatsu and N. Sawaki, J. Cryst. Growth 144 133 (1994).

15. S. Nakamura, Semicond. Sci. Technol. 14 R27 (1999).

16. C. Kisielowski, Z. Lileental-Weber and S. Nakamura, Jpn. J. Appl. Phys. 36 6932 (1997).

17. I. Akasaki, H. Amano, Y. Kiode, K. Hiramatsu and N. Sawaki, J. Cryst. Growth 98 209 (1989).

18. J. I. Pankove, S. Bloom and G. Harbeke, RCA Rev. 36 163 (1995).

19. R. J. Molnar,T. Lei and T. D. Moustakas, Appl. Phys. Lett. 62 72 (1993).

20. P. Boguslavski, E. L. Briggs and J. Bernholc, Phys. Rev. B51 17255 (1995).

21. D. W. Jenkins, J. D. Dow and M. H. Tsai, J. Appl. Phys. 72 4130 (1992).

22. B. V. Spitsyn, G. Popovici and M. A. Prelas, 2nd Int Conf. On the Applications of Diamond Films and Related Materials. ed. M.Yoshikawa et al. Tokyo: MYU (1993).

23. G. Popovici and H. Morkoc, GaN and Related Materials II. Ed. S. J. Pearton, NY: Gordon and Breach (2000).

24. J. A. Van Vechten, J. D. Zook, R. D. Honig and B. Goldenberg, Jpn. J. Appl. Phys. 31 3662 (1992).

25. J. Neugebauer and C. G. Van der Walle, Appl. Phys. Lett. 68 1829 (1995).

26. W. Gotz, N. M. Johnson, D. P. Bour, M. D. McCluskey and E. E. Haller, Appl. Phys. Lett. 69 3725 (1996).

27. W. Gotz, N. M. Johnson, D. P. Bour, C. Chen, C. Kuo, H. Liu and W. Imler, Proc. Electrochem. Soc. 96-11 87 (1996).

28. S. Nakamura, T. Mukai, M. Senoh and N. Iwasawa, Jpn. J. Appl. Phys. 31 L139 (1992).

29. W. Gotz, N. M. Johnson, J. Walker, D. P. Bour and R. A. Street, Appl. Phys. Lett. 68 667 (1996).

30. W. Kim, A. Salvador, A. E. Botchkarev, O. Aktas, S. N. Mohammed and H. Morkoc, Appl. Phys. Lett. 69 559 (1996).

31. W. Weifert, R. Franzheld, E. Butter, H. Sobotta and V. Riede, Cryst. Res. Techn. 18 383 (1983).

32. B. C. Chung and M. Gershenzon, J. Appl. Phys. 72 651 (1992).

33. C. Wetzel, T. Suski, J. W. Ager, E. R. Weber, E. E. Haller, S. Fischer, B. K. Meyer, R. J. Molnar and P. Perlin, Phys. Rev. Lett. 78 3923 (1997).

34. C. G. Van de Walle, Phys. Rev. B 57 2033 (1998).

35. A. Rode, A. McCamant, G. McCormac and B. Vetanen, in: Int. Electron Devices Mtg. Tech. Digest. New York: IEEE (1982).

36. Y. D. Shen, M. R. Wilson, M. McGuire, D. A. Nelson and B. M. Welch, in: 9th GaAs IC Symp. Tech. Digest. New York: IEEE (1987).

37. TriQuint Semiconductor, IC Foundary Services Manual. (1986).

38. Vitesse Semiconductor Corp. Company Backgrounder. January (1991).

39. J. C. Zolper, Ion Implantation Advances in Group III-Nitride Semiconductors in: GaN and Related Materials II. ed. S. J. Pearton, NY: Gordon and Breach (2000).

40. M. A. Khan, A. Bhattarai, J. N. Kuznia and D. T. Olson, Appl. Phys. Lett. 63 1214 (1993).

41. B. L. Sharma, in: Semiconductors and Semimetals: Contacts, Junctions, emitters. Vol. 15, eds. R. K. Willardson and A. C. Beer, New York: Academic (1981).

42. J. F. Gibbons, Proc. IEEE 56 295 (1968).

43. H. Ishiwara and S. Horita, Jap. J. Appl. Phys. 24 568 (1985).

44. H. H. Tan, J. S. Williams, C. Yuan and S. J. Pearton, Conf. Proc. MRS, Symposium AAA. Pittsburgh: Materials Research Society (Fall 1995).

45. H. H. Tan, J. S. Williams, J. Zou, D. J. H. Cockayne, S. J. Pearton and R. A. Stall, Appl. Phys. Lett. 69 2364 (1996).

46. H. P. Maruska and J. J. Tietjen, Appl. Phys. Lett. 15 327 (1969).

47. J. Neugebauer and C. G. Van de Walle, Appl. Phys. Lett. 69 503 (1996).

48. J. Neugebauer and C. G. Van de Walle, Phys. Rev. B 50 8067 (1994).

49. J. Neugebauer and C. G. Van de Walle, Appl. Proc. Int'l Conf. on the Physics of Semiconductors ICPS-22. Singapore: World Scientific (1995).

50. P. Perlin, T. Suzuki, H. Teisseyre, M. Leszczynski, I. Gregory, J. Jun, S. Porowski, P. Boguslawski, J. Bernholc, J. C. Chervin, A. Polian and T. D. Moustakas, Phys. Rev. Lett. 75 296 (1995).

51. C. Wetzel, W. Walukiewicz, E. E. Haller and J. Ager III, Phys. Rev. B 53 1322 (1996).

52. C. Wetzel, T. Suchi, J. W. Ager III, E. R. Weber, E. E. Haller, S. Fischer, B. K. Meyer. R. J. Molnax and P. Berlin, Phys. Rev. Lett. 78 3923 (1997).

53. J. C. Zolper, M. H. Crawford, H. H. Tan, J. X. Williams, J. Zhou, D. J. H. Cockayne, S. J. Pearton and R. F. Karlicek Jr. Appl. Phys. Lett. 70 2729 (1997).

54. J. C. Zolper, D. J. Rieger, A. G. Baca, S. J. Pearton, J. W. Lee and R. A. Stall, Appl. Phys. Lett. 69 538 (1996).

55. J. R. Mileham, S. J. Pearton, C. R. Abernathy, J. D. Mackenzie, R. J. Shul and S. P. Kilcoyne, Appl. Phys. Lett. 67 1119 (1995).

56. J. R. Mileham, S. J. Pearton, C. R. Abernathy, J. D. Mackenzie, R. J. Shul and S. P. Kilcoyne, J. Vac. Sci. Tech. B (in press).

57. S. J. Pearton and R. Caruso, Appl. Phys. Lett. 66 663 (1989).

58. J. hong, J. W. Lee, J. D. Mackenzie, S. M. Donovan, C. R. Abernathy, S. J. Pearton and J. C. Zolper, Semicond. Sci. Technol. 12 1310 (1997).

59. F. Ponce and D.P. Bour, Nature 386 351 (1997).

60. H. Morkoc, Nitride Semiconductors and Devices. Berlin: Springer-Verlag (1999).

61. T. Mori, T. Kozawa, T. Ohwaki and Y. Taga, Appl. Phys. Lett. 69 3537 (1996).

62. H. Ishikawa, S. Kobayashi and Y. Koide, J. Appl. Phys. 81 1315 (1997).

63. J. S. Jang, I. S. Chang, H. K. Kim, T. Y. Seong, S. Lee and S. J. Park, Appl. Phys. Lett. 74 70 (1999).

64. K. Kumakura and N. Kobayashi, Jap. J. Appl. Phys. 38 L1012 (1999).

65. P. Kozodoy, M. Hansen, S. P. DenBaars and U. K. Mishra, Appl. Phys. Lett. 74 3681 (1999).

66. P. Kozodoy, Y. Smorchkova, M. Hansen, H. Xing, S. P. DenBaars, U. K. Mishra, A. W. Saxler, R. Perrin and W. C. Mitchel, Appl. Phys. Lett. 75 2444 (1999).

67. E. F. Schubert, W. Grieshaber and I. D. Goepfert, Appl. Phys. Lett. 69 3737 (1996).

68. L. Hsu and W. Walukiewicz, Appl. Phys. Lett. 74 2405 (1999).

69. A. Saxler, W. C. Mitchel, P. Kung and M. Razeghi, Appl. Phys. Lett. 74 2023 (1993).

70. I. D. Goepfert, E. F. Schubert, A. Osinsky and P. E. Norris, Electron. Lett. 34 1109 (1999).

71. Y. L. Li, E. F. Schubert, W. Graff, A. Osinsky and W. F. Schaff, Appl. Phys. Lett. 76 2728 (2000).

72. P. M. Asbeck, E. T. Yu, S. S. Lau, G. J. Sullivan, J. VanHove and J. M. Redwing, Electron. Lett. 33 1230 (1997).

73. E. T. Yu, X. Z. Dang, P. M. Asbeck and S. S. Lau, J. Vac. Sci. Technol. B 17 1742 (1999).

74. O. Ambacher. J. Smart, J. R. Shealy, N. G. Weimann, K. Chu, M. Murphy, W. J. Schaff and L. F. Eastman, J. Appl. Phys. 85 3222 (1999).

75. I. D. Goepfert, E. F. Schubert, A. Osinsky, P.E. Norris and N. N. Faleev, J. Appl. Phys. 88 2030 (2000).

76. K. Kumakura, T. Makimato and N. Kobayashi, Jap. J. Appl. Phys, 39 L195 (2000).

77. K. Kumakura, T. Makimato and N. Kobayashi, Mat. Res. Soc. Symp. Proc 622 T5.11.1 (2000).

78. B. Meusching, C. Liv, B. Rauschenback, K. Kormitzer and W. Ritter, Mat. Sci. Eng. B 50 105 (1997).

79. J. C. Zolper, R. G. Wilson, S. J. Pearton and R. A. Stall, Appl. Phys. Lett. 68 1945 (1996).

80. S. J. Pearton, C. B. Vartuli, J. C. Zolper, C. Yuan and R. A. Stall, Appl. Phys. Lett. 67 1435 (1995).

81. J. S. Chan, N. W. Cheung, L. Schloss, E. Jones, W. S. Wong, X. Liu, E. R. Weber, A. Gassman and M. D. Rubin, Appl. Phys. Lett. 68 2702 (1996).

82. H. Kobayashi and W. M. Gibson, Appl. Phys. Lett. 74 2355 (1999).

83. H. H. Tan, J. S. Williams, J. Zou, D. J. H. Cockayne, S. J. Pearton, J. C. Zolper and R. A. Stall, Appl. Phys. Lett. 72 1190 (1998).

84. S. Strite, A. Pelzmann, T. Suski, M. Leszczynski, J. Jun, A. Rockett, M. Kamp and K. J. Ebeling. MRS Internet J. Nitride Semicond. Res. 2 15 (1997).

85. J. S. Williams, Mat. Sci. Eng. A 253 8 (1998).

86. S. O. Kucheyev, J. S. Williams, C. Jagadish, J. Zou, V. S. J. Craig and G. Li, Appl. Phys. Lett. 77 1455 (2000).

87. S. O. Kucheyev, J. S. Williams, C. Jagadish, J. Zou and G. Li, Phys. Rev. B 62 7510 (2000).

88. T. Yamamoto and H. Katayama-Yoshida, Jap. J. Appl. Phys. 36 L180 (1997).

89. T. Yamamoto and Y. Katayama-Yoshida, Mat. Sci. Forum 258-253 1185 (1997).

90. H. Reiss, C. S. Fuller and F. J. Morin, Bell Syst. Tech. J. 38 535 (1956).

91. O. Brandt, H. Yang, H. Kostial and K. H. Ploog, Appl. Phys. Lett. 69 2707 (1996).

92. B. Skromme and G. L. Martinez, Mat. Res. Soc. Symp. Vol. 595 W9.8.1 (2000).

93. Y. Sun, L. S. Tan, S. J. Chua and S. Prakash, Mat. Res. Soc. Symp. Proc. 595 W3.82.1 (2000).

94. F. Bernandini, V. Fiorentini and A. Bosin, Appl. Phys. Lett. 20 2990 (1990).

95. R. J. Shul, ICP Etching of GaN and Related Alloys, in: GaN and Related Materials II. ed. S. J. Pearton, NY: Gordon and Breach, (1999).

96. C. R. Eddy, Jr. and B. Molnar, J. Electron. Mater. 28, 314 (1999).

97. A. T. Ping, Q. Chen, J. W. Yang, M. A. Khan and I. Adesida, J. Electron. Mater. 27, 261 (1998)

98. I. Adesida, in ed. J. H. Edgar, S. Strite, H. Amano and I. Akasaki, London: Inspec (1999).

99. X. A. Cao, A. P. Zhang, G. T. Dang, H. Cho, F. Ren, S. J. Pearton, R. J. Shul, L. Zhang, R. Hickman and J. M. Van Hove, J. Vac. Sci. Tech. B. 17, 1540 (1999).

100. Z. F. Fan, S. N. Mohammed, W. Kim, O. Aktus, A. E. Botcharev and H. Morkoc, Appl. Phys. Lett. 69, 1672 (1996).

101. J. Y. Chen, C. J. Pan and G. C. Chi, Solid-State Electron., 43, 649 (1999).

102. X. A. Cao, S. J. Pearton, A. P. Zhang, G. T. Dang, F. Ren, R. J. Shul, L. Zhang, R. Hickman and J. M. Van Hove, Appl. Phys. Lett. 75, 2569 (1999).

103. W. A. Harrison, Electronic Structure and Properties of Solids. San Francisco: Freeman, (1980).

104. X. A. Cao, A. P.Zhang, G. T. Dang, H. Cho, F. Ren, S. J. Pearton, R. J. Shul, L. Zhang, R. Hickman and J. M. Van Hove, J. Vac. Sci. Tech. B 17, 1540 (1999).

105. J.Y. Chen, C.J. Pan and G.C. Chi, Solid-State Electron., 43, 649 (1999).

106. X. A. Cao, S. J. Pearton, A. P. Zhang, G. T. Dang, F. Ren, R. J. Shul, L. Zhang, R. Hickman and J. M. Van Hove, Appl. Phys. Lett. 75, 232 (1999).

107. X. A. Cao, S. J. Pearton, A. P. Zhang, G. T. Dang, F. Ren, R. J. Shul, L. Zhang, R. Hickman and J. M. Van Hove, Appl. Phys. Lett. 75, 2569 (1999).

108. A. J. Ping, A. C. Schmitz, I. Adesida, M. A. Khan, Q. Chen and Y. W. Yang, J. Electron Mater. 26, 266 (1997).

109. R. J. Shul, L. Zhang, A. G. Baca, C. G. Willison, J Han, S. J. Pearton, F. Ren, J. C. Zolper and L. F. Lester, Mat. Res. Soc. Symp. Proc. Vol. 573, 161 (1999).

110. R. J. Shul, L. Zhang, A. G. Baca, C. G. Willison, J. Han, S. J. Pearton and F. Ren, J. Vac. Sci. Technol. A 18, 1139 (2000).

111. C. Youtsey and I. Adesida in: Properties and Applications of GaN and Related Semiconductors. ed. J. H. Edgar, S. Strite, I. Akasaki, H. Amano and C. Wetzel, EMIS Data Reviews No. 23, London: INSPEC, IEE (1999).

112. B. J. Kim, J. W. Lee, H. S. Park, Y. Park and T. I. Kim, J. Electron. Mater. 27 L32 (1998).

113. J. M. Lee, K. M. Chang, S. W. Kim, C. Huh, I. H. Lee and S. J. Park, J. Appl. Phys. 87, 7667 (2000).

114. J. R. Mileham, S. J. Pearton, C. R. Abernathy, J. D. Mackenzie, R. J. Shul and S. P. Kilcoyne, J. Vac. Sci. Tech. A. 14, 836 (1996).

115. D. A. Stocker, E. F. Schubert and J. M. Redwing, Appl. Phys. Lett. 73 2345 (1998).

116. R. J. Shul, G. B. McClellan, S. J. Pearton, C. R. Abernathy, C. Constantine and C. Barratt, Electron. Lett. 32 1408 (1996).

117. R. J. Shul, G. B. McClellan, S. A. Casalnuovo, D. J. Rieger, S. J. Pearton, C. Constantine, C. Barratt, R. F. Karlicek, Jr., C. Tran and M. Schurman, Appl. Phys. Lett. 69 1119 (1996).

118. K. K. Ko, S. W. Pang, T. Brock, M. W. Cole and L. M. Casas, J. Vac. Sci. Technol. B 12 3382 (1994).

119. R. J. Davis and P. Jha, J. Vac. Sci. Technol. B 13 242 (1995).

120. K. T. Sung, S. W. Pang, M. W. Cole and N. Pearce, J. Electrochem. Soc. 142 206 (1995).

121. A. S. Yapsir, G. Fortuno-Wiltshire, J. P. Gambino, R. H. Kastl and C. C. Parks, J. Vac. Sci. Technol. A 8 2939 (1990).

122. I-Wen H. Connick, A. Bhattacharyya and K. N. Ritz, J. Appl. Phys. 64 2059 (1988).

123. O. W. Purbo, R. R. Selvakumar and D. Misra, J. Electrochem. Soc. 140 2659 (1993).

124. K. T. Sung and S. W. Pang, J. Vac. Sci. Technol. A 12 1346 (1994).

125. J. Asmussen, J. Vac. Sci. Technol. A 7 883 (1989).

126. S. Nakayama, Pure Appl. Chem. 62 1751 (1990).

127. H. J. Kijkstra, J. Vac. Sci. Technol. B 10 2222 (1992).

128. S. W. Pang in: Handbook of Advanced Plasma Processing Techniques. eds. R. J. Shul and S. J. Pearton, Berlin: Springer-Verlag, (2000).

129. X. A. Cao, Advanced Processing of GaN for Novel Electronic Devices. PhD Dissertation, Gainesville: University of Florida, (2000).

130. J.I. Pankove, J.T. Torvik, C.H. Qiu, I. Grzegory, S. Porwski, P. Quigley and B. Martin. Appl. Phys. Lett. 74 416 (1999).

131. J. P. Biersack and J. F. Ziegler, The Stopping and Range of Ions in Matter. July 2000. (1999).<http:www.research.ibm.com/ionbeams/>.

132. D.J. Dewsnip, A.V. Andrianov, I. Harrison, J.W. Orton, D.E. Lacklison, G.B. Ren, S.E. Hopper, J.S. Cheng and C.T. Foxon, Semicond. Sci. Techn. 13 500 (1998).

133. F.J. Sanchez, F. Calle, M.A. Sanchez-Garcia, E. Calleja, E. Munoz, C.H. Molly, D.J. Somerford, F.K. Koschnik, K. Michael and J.M. Spaeth, MRS Internet J. Nitride Semicond. Res. 3 19 (1998).

APPENDIX

The stopping and range of ions in matter (SRIM) simulator was used to calculate the implanted ranges and ion distribution of Be, Mg, and O in GaN.[131]

Table 3 Be in GaN

Target = Beryllium in Ga-N
Density = 6.1000E+00 g*cm^{-3} = 8.7748E+22 atoms*cm^{-3}

======= Target Composition ========

Atom Name	Atom Numb	Atomic Percent	Mass Percent
Ga	31	050.00	083.27
N	7	050.00	016.73

====================================

Stopping Units = eV / Angstrom

Ion = Beryllium [4] , Mass = 9.012 amu

Ion Energy	dE/dx Elec.	dE/dx Nuclear	Projected Range	Longitudinal Straggling	Lateral Straggling
10.00 keV	9.596E+00	8.339E+00	263 A	209 A	160 A
11.00 keV	1.004E+01	8.153E+00	289 A	226 A	173 A
12.00 keV	1.045E+01	7.975E+00	315 A	243 A	187 A
13.00 keV	1.086E+01	7.806E+00	341 A	259 A	200 A
14.00 keV	1.124E+01	7.645E+00	367 A	275 A	213 A
15.00 keV	1.161E+01	7.492E+00	394 A	291 A	225 A
16.00 keV	1.197E+01	7.345E+00	420 A	306 A	238 A
17.00 keV	1.231E+01	7.206E+00	447 A	321 A	250 A

18.00 keV	1.265E+01	7.072E+00	473 A	336 A	263 A
20.00 keV	1.329E+01	6.823E+00	527 A	365 A	287 A
22.50 keV	1.405E+01	6.540E+00	594 A	400 A	317 A
25.00 keV	1.476E+01	6.284E+00	661 A	434 A	346 A
27.50 keV	1.544E+01	6.051E+00	728 A	466 A	374 A
30.00 keV	1.608E+01	5.839E+00	796 A	498 A	401 A
32.50 keV	1.670E+01	5.644E+00	863 A	528 A	428 A
35.00 keV	1.729E+01	5.464E+00	930 A	558 A	455 A
37.50 keV	1.786E+01	5.297E+00	997 A	586 A	480 A
40.00 keV	1.841E+01	5.143E+00	1065 A	614 A	505 A
45.00 keV	1.946E+01	4.864E+00	1198 A	666 A	554 A
50.00 keV	2.045E+01	4.619E+00	1331 A	715 A	601 A
55.00 keV	2.138E+01	4.402E+00	1463 A	762 A	646 A
60.00 keV	2.228E+01	4.208E+00	1594 A	806 A	689 A
65.00 keV	2.313E+01	4.034E+00	1724 A	848 A	731 A
70.00 keV	2.395E+01	3.875E+00	1853 A	888 A	771 A
80.00 keV	2.550E+01	3.599E+00	2107 A	961 A	848 A
90.00 keV	2.695E+01	3.366E+00	2357 A	1029 A	920 A
100.00 keV	2.832E+01	3.165E+00	2602 A	1091 A	988 A
110.00 keV	2.961E+01	2.990E+00	2843 A	1148 A	1051 A
120.00 keV	3.089E+01	2.836E+00	3080 A	1201 A	1112 A
130.00 keV	3.212E+01	2.700E+00	3312 A	1250 A	1169 A
140.00 keV	3.333E+01	2.578E+00	3540 A	1296 A	1223 A
150.00 keV	3.450E+01	2.468E+00	3764 A	1338 A	1274 A
160.00 keV	3.578E+01	2.368E+00	3984 A	1378 A	1324 A
170.00 keV	3.708E+01	2.278E+00	4198 A	1415 A	1370 A
180.00 keV	3.837E+01	2.195E+00	4408 A	1450 A	1415 A
200.00 keV	4.093E+01	2.048E+00	4815 A	1514 A	1497 A
225.00 keV	4.410E+01	1.892E+00	5299 A	1583 A	1590 A
250.00 keV	4.726E+01	1.762E+00	5759 A	1643 A	1674 A
275.00 keV	5.042E+01	1.650E+00	6196 A	1695 A	1748 A
300.00 keV	5.340E+01	1.554E+00	6614 A	1741 A	1816 A

Table 4 Mg in GaN

Target = Magnesium in Ga-N
Density = 6.1000E+00 g/cm3 = 8.7748E+22 atoms/cm3
======= Target Composition ========

Atom Name	Atom Numb	Atomic Percent	Mass Percent
Ga	31	050.00	083.27
N	7	050.00	016.73

====================================

Stopping Units = eV / Angstrom

Ion = Magnesium [12] , Mass = 23.985 amu

Ion Energy	dE/dx Elec.	dE/dx Nuclear	Projected Range	Longitudinal Straggling	Lateral Straggling
10.00 keV	9.276E+00	5.091E+01	104 A	72 A	53 A
11.00 keV	9.701E+00	5.109E+01	113 A	78 A	57 A
12.00 keV	1.011E+01	5.119E+01	122 A	83 A	61 A
13.00 keV	1.049E+01	5.123E+01	130 A	89 A	65 A
14.00 keV	1.087E+01	5.122E+01	139 A	94 A	68 A
15.00 keV	1.122E+01	5.117E+01	148 A	99 A	72 A
16.00 keV	1.157E+01	5.109E+01	157 A	104 A	76 A
17.00 keV	1.190E+01	5.098E+01	165 A	110 A	80 A
18.00 keV	1.223E+01	5.085E+01	174 A	115 A	84 A
20.00 keV	1.285E+01	5.053E+01	192 A	125 A	91 A
22.50 keV	1.358E+01	5.007E+01	214 A	138 A	100 A
25.00 keV	1.427E+01	4.956E+01	236 A	151 A	110 A
27.50 keV	1.492E+01	4.902E+01	259 A	164 A	119 A
30.00 keV	1.555E+01	4.846E+01	282 A	176 A	128 A
32.50 keV	1.614E+01	4.789E+01	305 A	189 A	137 A
35.00 keV	1.671E+01	4.732E+01	328 A	202 A	146 A
37.50 keV	1.727E+01	4.675E+01	351 A	214 A	156 A
40.00 keV	1.780E+01	4.619E+01	374 A	227 A	165 A
45.00 keV	1.881E+01	4.510E+01	422 A	251 A	183 A
50.00 keV	1.976E+01	4.404E+01	470 A	276 A	201 A
55.00 keV	2.067E+01	4.303E+01	518 A	301 A	220 A
60.00 keV	2.153E+01	4.206E+01	567 A	325 A	238 A
65.00 keV	2.236E+01	4.114E+01	617 A	349 A	256 A
70.00 keV	2.315E+01	4.026E+01	667 A	373 A	275 A
80.00 keV	2.465E+01	3.862E+01	769 A	421 A	312 A
90.00 keV	2.605E+01	3.713E+01	872 A	468 A	349 A
100.00 keV	2.738E+01	3.577E+01	977 A	514 A	385 A

110.00 keV	2.863E+01	3.452E+01	1083 A	559 A	422 A
120.00 keV	2.983E+01	3.337E+01	1190 A	604 A	459 A
130.00 keV	3.097E+01	3.231E+01	1298 A	648 A	495 A
140.00 keV	3.207E+01	3.133E+01	1407 A	692 A	532 A
150.00 keV	3.312E+01	3.041E+01	1516 A	734 A	568 A
160.00 keV	3.414E+01	2.956E+01	1627 A	776 A	604 A
170.00 keV	3.513E+01	2.877E+01	1737 A	818 A	640 A
180.00 keV	3.609E+01	2.802E+01	1849 A	858 A	675 A
200.00 keV	3.792E+01	2.665E+01	2073 A	937 A	746 A
225.00 keV	4.008E+01	2.516E+01	2354 A	1032 A	833 A
250.00 keV	4.211E+01	2.385E+01	2636 A	1123 A	918 A
275.00 keV	4.402E+01	2.269E+01	2919 A	1211 A	1002 A
300.00 keV	4.618E+01	2.165E+01	3201 A	1295 A	1083 A

Table 5 O in GaN

Target = Oxygen in Ga-N
Density = 6.1000E+00 g*cm^{-3} = 8.7748E+22 atoms*cm^{-3}

======= Target Composition ========

Atom Name	Atom Numb	Atomic Percent	Mass Percent
Ga	31	050.00	083.27
N	7	050.00	016.73

====================================

Stopping Units = eV / Angstrom

Ion = Oxygen [8] , Mass = 15.995 amu

Ion Energy	dE/dx Elec.	dE/dx Nuclear	Projected Range	Longitudinal Straggling	Lateral Straggling
10.00 keV	1.442E+01	2.717E+01	137 A	99 A	74 A
11.00 keV	1.508E+01	2.700E+01	149 A	107 A	80 A
12.00 keV	1.571E+01	2.681E+01	161 A	115 A	86 A
13.00 keV	1.631E+01	2.660E+01	173 A	122 A	91 A
14.00 keV	1.689E+01	2.638E+01	185 A	129 A	97 A
15.00 keV	1.745E+01	2.616E+01	197 A	137 A	102 A
16.00 keV	1.799E+01	2.593E+01	210 A	144 A	108 A
17.00 keV	1.851E+01	2.571E+01	222 A	151 A	113 A
18.00 keV	1.901E+01	2.548E+01	234 A	158 A	119 A
20.00 keV	1.997E+01	2.502E+01	259 A	172 A	130 A
22.50 keV	2.111E+01	2.447E+01	290 A	189 A	143 A
25.00 keV	2.218E+01	2.393E+01	321 A	206 A	156 A
27.50 keV	2.320E+01	2.341E+01	352 A	222 A	169 A
30.00 keV	2.417E+01	2.292E+01	383 A	238 A	182 A
32.50 keV	2.509E+01	2.244E+01	414 A	254 A	194 A
35.00 keV	2.598E+01	2.199E+01	445 A	270 A	207 A
37.50 keV	2.684E+01	2.155E+01	477 A	285 A	219 A
40.00 keV	2.767E+01	2.114E+01	508 A	300 A	231 A
45.00 keV	2.924E+01	2.036E+01	571 A	329 A	255 A
50.00 keV	3.073E+01	1.965E+01	635 A	357 A	279 A
55.00 keV	3.213E+01	1.900E+01	698 A	384 A	302 A
60.00 keV	3.348E+01	1.839E+01	761 A	411 A	324 A
65.00 keV	3.476E+01	1.783E+01	825 A	436 A	347 A
70.00 keV	3.599E+01	1.731E+01	888 A	461 A	368 A
80.00 keV	3.832E+01	1.637E+01	1014 A	509 A	411 A
90.00 keV	4.050E+01	1.555E+01	1140 A	554 A	452 A
100.00 keV	4.256E+01	1.482E+01	1265 A	596 A	491 A

110.00 keV	4.451E+01	1.417E+01	1389 A	637 A	530 A
120.00 keV	4.637E+01	1.358E+01	1513 A	675 A	567 A
130.00 keV	4.815E+01	1.305E+01	1635 A	712 A	602 A
140.00 keV	4.985E+01	1.256E+01	1756 A	747 A	637 A
150.00 keV	5.149E+01	1.212E+01	1877 A	780 A	671 A
160.00 keV	5.308E+01	1.171E+01	1997 A	812 A	703 A
170.00 keV	5.462E+01	1.134E+01	2115 A	843 A	735 A
180.00 keV	5.610E+01	1.099E+01	2233 A	872 A	766 A
200.00 keV	5.910E+01	1.036E+01	2464 A	927 A	825 A
225.00 keV	6.276E+01	9.684E+00	2748 A	990 A	895 A
250.00 keV	6.630E+01	9.104E+00	3024 A	1048 A	960 A
275.00 keV	6.987E+01	8.599E+00	3293 A	1100 A	1021 A
300.00 keV	7.413E+01	8.155E+00	3554 A	1148 A	1077 A

Multiply Stopping by	for Stopping Units
1.0000E+00	eV / Angstrom
1.0000E+01	keV / micron
1.0000E+01	MeV / mm
1.6394E-02	keV / (ug/cm2)
1.6394E-02	MeV / (mg/cm2)
1.6394E+01	keV / (mg/cm2)
1.1396E+00	eV / (1E15 atoms/cm2)
3.1062E-02	L.S.S. reduced units

BIOGRAPHICAL SKETCH

Donald G. Kent III was born in Washington D.C. June 16, 1967. Upon completing high school he attended Daytona Beach Community College. While in the final semester of his two-year Associates program, he withdrew from classes and moved to Hawaii to own and operate a contracting business, which lasted for six years. He moved back to Florida in the summer of 1995 with the intention of finishing his education. Don matriculated at the University of Florida in December of 1996; he was conferred the degree of Bachelor of Science in Chemical Engineering with a minor in Materials Science and Engineering in December of 1999. His interest in Electronic Materials spurred him to graduate school. Don will graduate with his Masters degree in Materials Science and Engineering in May 2001. While under the tutelage of Dr. Stephen J. Pearton, he has had the opportunity to work on several projects relating to the processing of Gallium Nitride. He has attended and given presentations of his research to two MRS conferences, and has authored several technical papers. Don is a member of Tau Beta Pi, the American Institute of Chemical Engineers, the American Chemical Society, and the Materials Research Society.